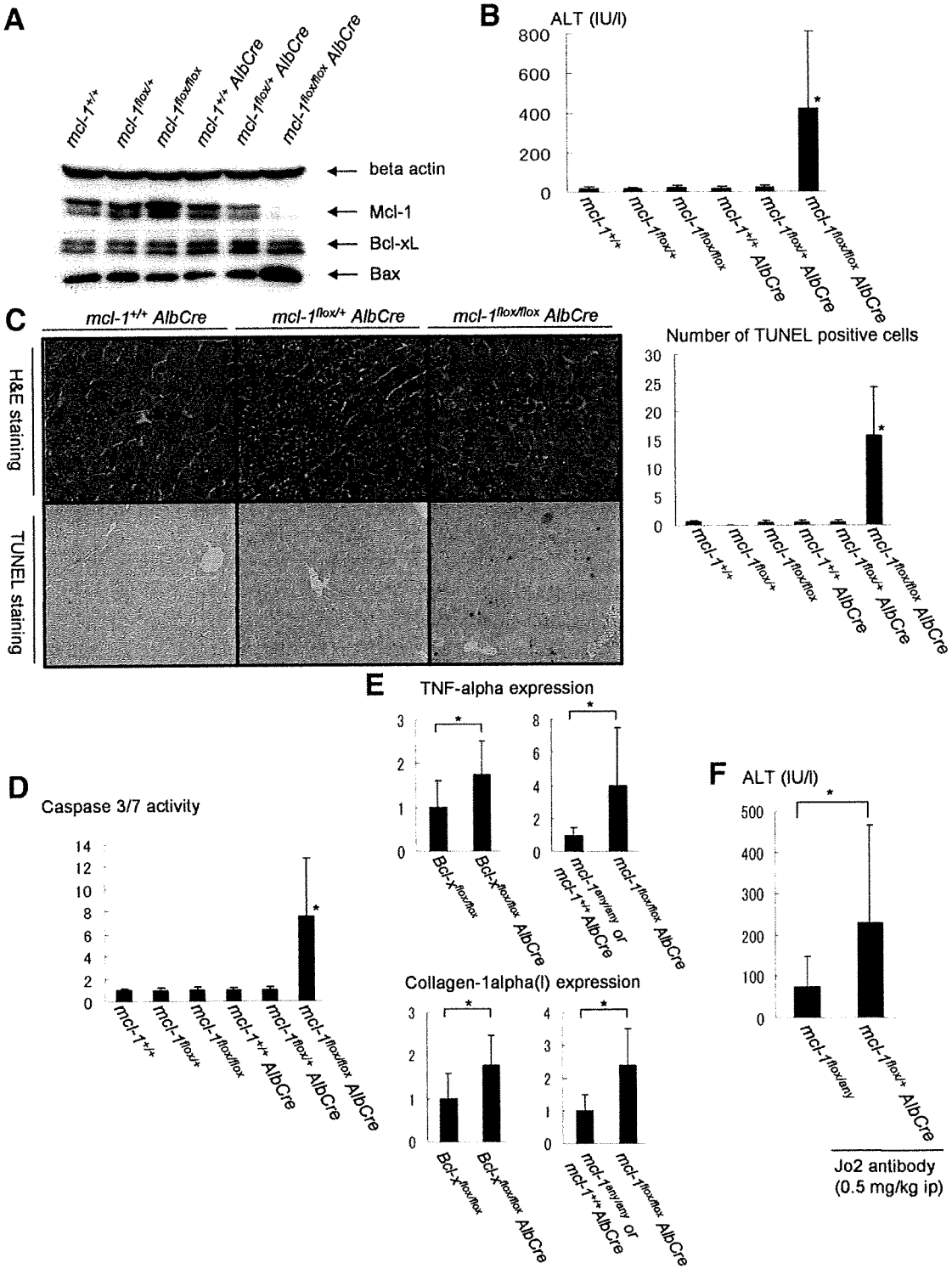

Fig. 1. Hepatocyte-specific Mcl-1 knockout mice. Offspring from mating of *mcl-1*$^{flox/+}$ *AlbCre* mice and *mcl-1*$^{flox/+}$ mice were sacrificed at the age of 6 weeks. (A) Western blot of whole liver lysate for the expression of Bcl-xL, Mcl-1, and Bax. (B) Serum ALT levels. N = 15 mice for each group. *$P < 0.05$ versus the other five groups. (C) Left panel shows hematoxylin-eosin and TUNEL staining of the liver section. Arrow indicates typical apoptotic cells. Right panel shows statistics of TUNEL-positive cells. The number of TUNEL-positive cells was determined in a defined area. N = 5 mice for each group. *$P < 0.05$ versus the other five groups. (D) Serum levels of caspase-3/7 activity. The levels were normalized to *mcl-1*$^{+/+}$ *AlbCre* (−) mice. N = 15 mice for each group. *P < 0.05 versus the other five groups. (E) Real-time RT-PCR analysis for TNF-α and collagen-1alpha(1) expression. *$P < 0.05$. N = 12 or 9. The levels were normalized to the wild-type mice. (F) Serum ALT levels of Fas-stimulated mice. The *mcl-1*$^{flox/+}$ *AlbCre* mice and *mcl-1*$^{flox/+ \text{ or } flox}$ mice were sacrificed 3 hours after intraperitoneal injection of 0.5 mg/kg Jo2 antibody. *$P < 0.05$. N = 13 or 7.

Therefore, we examined the susceptibility to Fas stimulation in these mice. We injected anti-Fas antibody into *mcl-1*$^{flox/+}$ *AlbCre* mice and *mcl-1*$^{flox/+\ or\ flox}$ mice and measured the levels of their serum ALT. *mcl-1*$^{flox/+}$ *AlbCre* mice displayed significantly higher levels of serum ALT than control mice (Fig. 1F). These findings suggest that haplo-deficiency of Mcl-1 does not produce apoptosis in a physiological setting but clearly reduces apoptosis resistance under pathological conditions.

Involvement of Bid in Apoptosis Caused by Mcl-1 Deficiency. BH3-only proteins regulate life and death balance by interacting with core Bcl-2 family members. The hepatocyte is a so-called type 2 cell, which requires Bid as a sensor for Fas-mediated apoptotic stresses.[19] In addition, it has been reported that the caspase-8/Bid pathway is involved in a variety of liver pathological conditions.[16,20] To examine the possibility of Bid being involved in hepatocyte apoptosis caused by Mcl-1 deficiency, we crossed hepatocyte-specific Mcl-1 knockout mice with Bid knockout mice. Offspring form mating of *bid*$^{+/-}$ *mcl-1*$^{flox/flox}$ *AlbCre* mice with *bid*$^{+/-}$ *mcl-1*$^{flox/flox}$ mice were sacrificed at 6 weeks after birth and subjected to analysis of apoptosis phenotypes. Mice with each genotype grew up, and, as expected, the levels of Bid and/or Mcl-1 expression in the liver were correspondingly reduced with their genotypes (Fig. 2A). The levels of serum ALT were significantly lower in *bid*$^{-/-}$ *mcl-1*$^{flox/flox}$ *AlbCre* mice than in *bid*$^{+/+}$ *mcl-1*$^{flox/flox}$ *AlbCre* mice (Fig. 2B). The results indicate that Bid was involved in hepatocyte apoptosis found in Mcl-1 knockout mice.

Combined Deficiency of Mcl-1 and Bcl-xL in Hepatocytes Causes Lethality. Phenotypes observed in hepatocyte-specific Mcl-1 knockout mice were very similar to those in hepatocyte-specific Bcl-xL knockout mice.[13] These results indicated that Bcl-xL and Mcl-1 share similar anti-apoptotic functions but do not compensate for the loss of each other. To examine whether their expression and function are completely nonredundant or just partially so, we generated hepatocyte-specific Bcl-xL/Mcl-1 double-knockout mice.

The *bcl-x*$^{flox/+}$ *mcl-1*$^{flox/+}$ *AlbCre* mice were mated with *bcl-x*$^{flox/flox}$ *mcl-1*$^{flox/flox}$ mice, and genotypes of the offspring were screened at 3 weeks after birth. *AlbCre*-negative and *bcl-x*$^{flox/+}$ *mcl-1*$^{flox/+}$ *AlbCre* mice were born and grew up, but not *bcl-x*$^{flox/flox}$ *mcl-1*$^{flox/+}$ *AlbCre*, *bcl-x*$^{flox/+}$ *mcl-1*$^{flox/flox}$ *AlbCre*, and *bcl-x*$^{flox/flox}$ *mcl-1*$^{flox/flox}$ *AlbCre* mice (Table 1). The lack of Bcl-xL and Mcl-1 caused a more severe phenotype than either knockout, suggesting that they partially compensate for the loss of each other at least from the viewpoint of maintaining normal development.

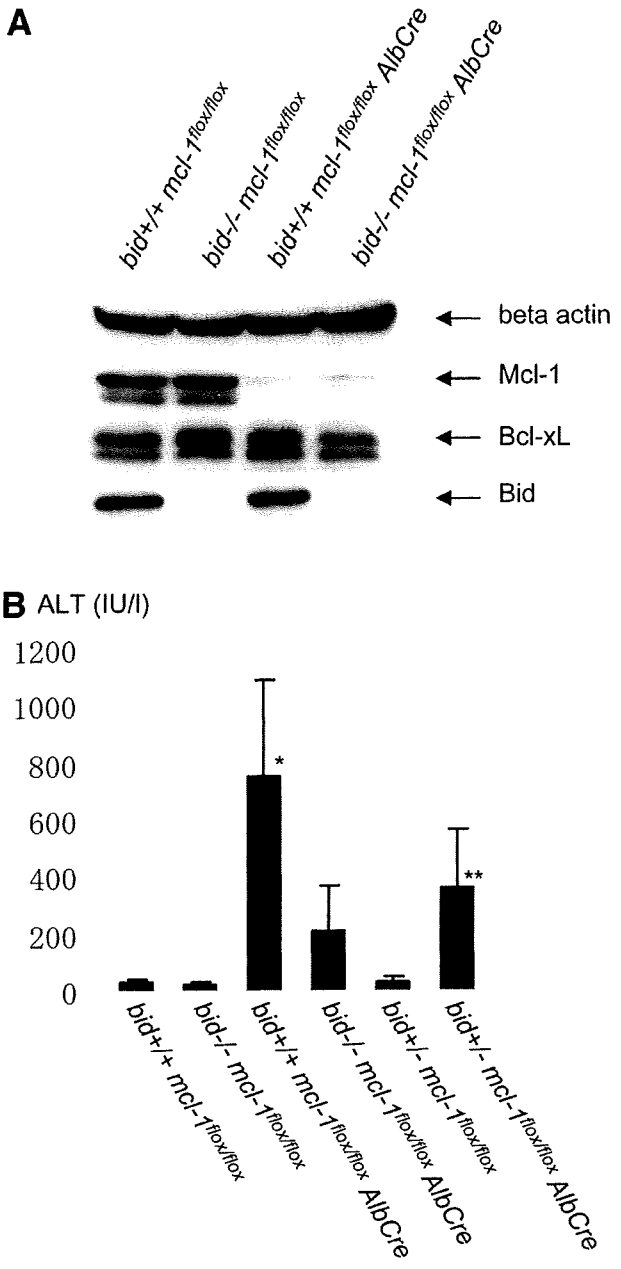

Fig. 2. Mcl-1/Bid double-knockout mice. Offspring from mating of *bid*$^{+/-}$ *mcl-1*$^{flox/flox}$ *AlbCre* mice with *bid*$^{+/-}$ *mcl-1*$^{flox/flox}$ mice were sacrificed at 6 weeks after birth. (A) Western blot of whole liver lysate for the expression of Mcl-1, Bcl-xL, and Bid. (B) Serum ALT levels. N = 12 mice for each group. *$P < 0.05$ versus the other five groups; **$P < 0.05$ versus the *AlbCre*-negative groups and the *bid*$^{+/+}$ *mcl-1*$^{flox/flox}$ *AlbCre* group.

Mice Lacking Single Alleles for Both Bcl-xL and Mcl-1 Develop Spontaneous Apoptosis in the Adult Liver Similar to Bcl-xL or Mcl-1 Knockout Mice. Offspring from mating of *bcl-x*$^{flox/+}$ *mcl-1*$^{flox/+}$ *AlbCre and bcl-x*$^{flox/flox}$ *mcl-1*$^{flox/flox}$ were sacrificed at 6 weeks after birth and subjected to analysis of Bcl-xL/Mcl-1 expression and

Table 1. Genotyping of Offspring Obtained by Crossing *bcl-x*$^{flox/+}$ *mcl-1*$^{flox/+}$ *AlbCre* Mice and *bcl-x*$^{flox/flox}$ *mcl-1*$^{flox/flox}$ Mice

AlbCre	bcl-x	mcl-1	ED18.5	3 Weeks
–	flox/+	flox/+	4	14
–	flox/flox	flox/+	6	17
–	flox/+	flox/flox	12	17
–	flox/flox	flox/flox	7	17
+	flox/+	flox/+	11	22
+	flox/flox	flox/+	8	0
+	flox/+	flox/flox	9	0
+	flox/flox	flox/flox	10	0
	Total		67	87

ED, embryonic day.
Note that each genotype is expected to account for one-eighth of the offspring from this mating.

apoptosis phenotypes. As expected, *bcl-x*$^{flox/+}$ *mcl-1*$^{flox/+}$ *AlbCre* liver expressed reduced levels of expression for both Bcl-xL and Mcl-1 (Fig. 3A). Interestingly, *bcl-x*$^{flox/+}$ *mcl-1*$^{flox/+}$ *AlbCre* mice developed spontaneous hepatocyte apoptosis as evidenced by an increase in serum ALT levels and caspase-3/7 activity (Fig. 3B,C). In agreement with this, hepatocytes with typical apoptotic morphology and positive for TUNEL staining were found scattered in the liver lobules in these mice (Fig. 3D,E). Furthermore, *bcl-x*$^{flox/+}$ *mcl-1*$^{flox/+}$ *AlbCre* mice showed higher expression of TNF-α than wild-type mice (Fig. 3F). The phenotypes were very similar to hepatocyte-specific Bcl-xL or Mcl-1knockout mice.

Hepatocyte-Specific Mcl-1/Bcl-xL-Deficient Mice Show Impaired Development of the Liver and Liver Failure During the Neonatal Period. To examine the impact of Bcl-xL/Mcl-1deficiency at an earlier time point, offspring obtained from crossing *bcl-x*$^{flox/+}$ *mcl-1*$^{flox/+}$ *AlbCre* mice and *bcl-x*$^{flox/flox}$ *mcl-1*$^{flox/flox}$ mice were analyzed on gestational day 18.5. Live-obtained embryo followed expected Mendelian frequencies (Table 1). Overall, they looked normal, and their body weight did not differ among genotypes (Fig. 4A,B). However, the livers obtained from live pups with genotype of *bcl-x*$^{flox/flox}$ *mcl-1*$^{flox/+}$ *AlbCre*, *bcl-x*$^{flox/+}$ *mcl-1*$^{flox/flox}$ *AlbCre*, or *bcl-x*$^{flox/flox}$ *mcl-1*$^{flox/flox}$ *AlbCre* were clearly smaller. The ratios of liver weight to body weight were significantly lower in those pups than in *AlbCre*-negative or *bcl-x*$^{flox/+}$ *mcl-1*$^{flox/+}$ *AlbCre* pups (Fig. 4C). The ratios of liver weight to body weight were also examined in *mcl-1*$^{flox/flox}$ with *AlbCre* or without *AlbCre* mice, and there was no significant difference between the two (6.0 ± 0.8 versus 5.5 ± 0.9, $N = 5$, $P = 0.34$), excluding the possibility that Mcl-1 knockout itself affects the liver size at this time point. Histological analysis revealed that there were a number of hepatocytes with rectangular morphology and hematopoietic cells in the developing liver of the *AlbCre*-negative pups (Fig. 4D). Whereas the number of rectangular hepatocytes in *bcl-x*$^{flox/+}$ *mcl-1*$^{flox/+}$ *AlbCre* livers was similar to that in the *AlbCre*-negative livers, it was lower in *bcl-x*$^{flox/flox}$ *mcl-1*$^{flox/+}$ *AlbCre*, *bcl-x*$^{flox/+}$ *mcl-1*$^{flox/flox}$ *AlbCre*, and *bcl-x*$^{flox/flox}$ *mcl-1*$^{flox/flox}$ *AlbCre* livers. Rectangular cells were rarely observed in *bcl-x*$^{flox/flox}$ *mcl-1*$^{flox/flox}$ *AlbCre* livers. Furthermore, the expression of albumin and transthyretin was examined in the liver as a marker for hepatocyte differentiation.[21] Consistent with histological findings, both expressions were gradually reduced from the *AlbCre*-negative livers to the *bcl-x*$^{flox/flox}$ *mcl-1*$^{flox/flox}$ *AlbCre* livers (Fig. 4E,F).

We noticed that offspring obtained from crossing *bcl-x*$^{flox/+}$ *mcl-1*$^{flox/+}$ *AlbCre* mice and *bcl-x*$^{flox/flox}$ *mcl-1*$^{flox/flox}$ mice frequently died within 1 day after birth. To examine the cause of the early neonatal death, offspring were sacrificed at 10 hours after birth. They were divided into two groups according to the data shown in Table 1: expected survivors including *AlbCre*-negative and *bcl-x*$^{flox/+}$ *mcl-1*$^{flox/+}$ *AlbCre* pups, and expected nonsurvivors including *bcl-x*$^{flox/flox}$ *mcl-1*$^{flox/+}$ *AlbCre*, *bcl-x*$^{flox/+}$ *mcl-1*$^{flox/flox}$ *AlbCre*, and *bcl-x*$^{flox/flox}$ *mcl-1*$^{flox/flox}$ *AlbCre* pups. The levels of total bilirubin and ammonia in circulation were determined and compared between the groups. Both blood bilirubin levels and ammonia levels were significantly higher in the expected nonsurvivors than in the expected survivors (Fig. 5A,B). These results suggested that *bcl-x*$^{flox/flox}$ *mcl-1*$^{flox/+}$ *AlbCre*, *bcl-x*$^{flox/+}$ *mcl-1*$^{flox/flox}$ *AlbCre*, and *bcl-x*$^{flox/flox}$ *mcl-1*$^{flox/flox}$ *AlbCre* mice died quickly after birth because of hepatic failure, in agreement with the findings of impaired liver development.

Discussion

Five members of the anti-apoptotic Bcl-2 family have been found: Bcl-2, Bcl-xL, Bcl-w, Bfl-1, and Mcl-1. Traditional knockout of Bcl-2, a prototype of this family, displays growth retardation, hair color abnormality, lymphocyte decrease, and polycystic kidney.[22,23] In agreement with the finding that Bcl-2 is not expressed in hepatocytes,[13] these mice did not show any liver phenotypes. Similarly, Bcl-w[24,25] or Bfl-1 knockout mice[26] were generated but no liver phenotypes have been reported. Traditional knockout of Bcl-xL or Mcl-1 caused more severe phenotypes. Deletion of the *bcl-x* gene resulted in embryonic lethality because of abnormal neuronal development and hematopoiesis.[27] The *mcl-1* knockout embryo fails to be implanted *in utero*.[28] Thus, study of traditional knockout mice could not reveal the significance of Bcl-xL or Mcl-1 in the liver.

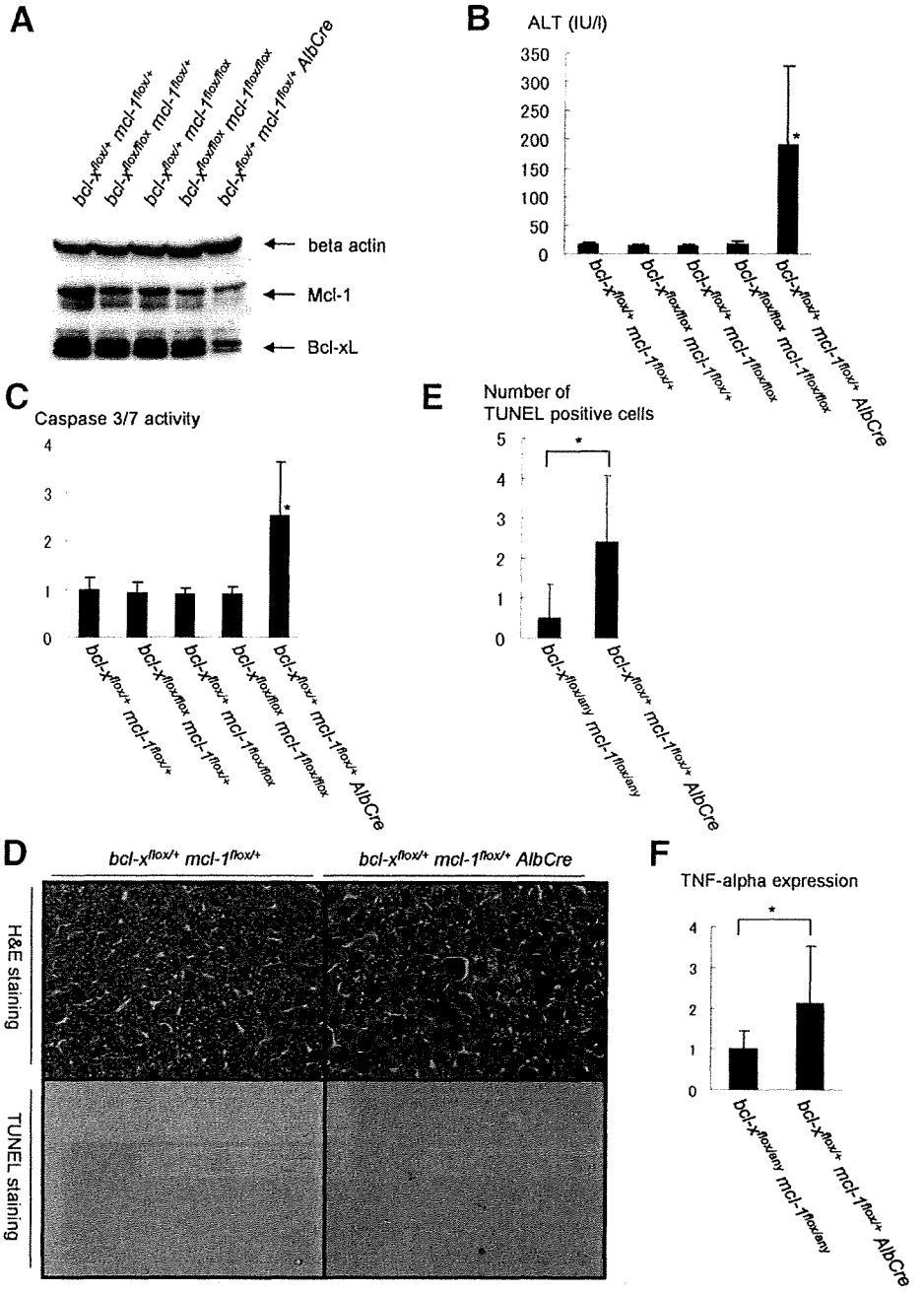

Fig. 3. Hepatocyte-specific Bcl-xL/Mcl-1-deficient mice. Offspring from mating *bcl-x*$^{flox/+}$ *mcl-1*$^{flox/+}$ *AlbCre* mice and *bcl-x*$^{flox/flox}$ *mcl-1*$^{flox/flox}$ mice were sacrificed at the age of 6 weeks. (A) Western blot of whole liver lysate for the expression of Bcl-xL and Mcl-1. (B) Serum ALT levels. N = 9 mice for each group. *$P < 0.05$ versus the other five groups. (C) Serum levels of caspase-3/7 activity. The levels were normalized to *bcl-x*$^{flox/+}$ *mcl-1*$^{flox/+}$ mice. N = 9 mice for each group. *$P < 0.05$ versus the other five groups. (D) Hematoxylin-eosin and TUNEL staining of the liver sections for *bcl-x*$^{flox/+}$ *mcl-1*$^{flox/+}$ *AlbCre* mice. Findings for *bcl-x*$^{flox/+}$ *mcl-1*$^{flox/+}$ mice are shown as a control. (E) Statistics of TUNEL-positive cells. The number of TUNEL-positive cells was determined in a defined area. N = 5 or 6. *$P < 0.05$. (F) RT-PCR analysis for TNF-α expression. The levels were normalized to the group of *bcl-x*$^{flox/+ \text{ or } flox}$ *mcl-1*$^{flox/+ \text{ or } flox}$. *$P < 0.05$. N = 9.

We previously reported that hepatocyte-specific knockout of Bcl-xL caused spontaneous apoptosis in hepatocytes after birth and established that Bcl-xL is critically important for the integrity of hepatocytes.[13] The current study demonstrated that Mcl-1 plays an anti-apoptotic role in differentiated hepatocytes similar to that of Bcl-xL. During the preparation of this manuscript, a report by Vick et al.[29] appeared on the Web, demonstrating a similar apoptosis phenotype in mice with specific knockout of the *mcl-1* gene in hepatocytes. Our findings

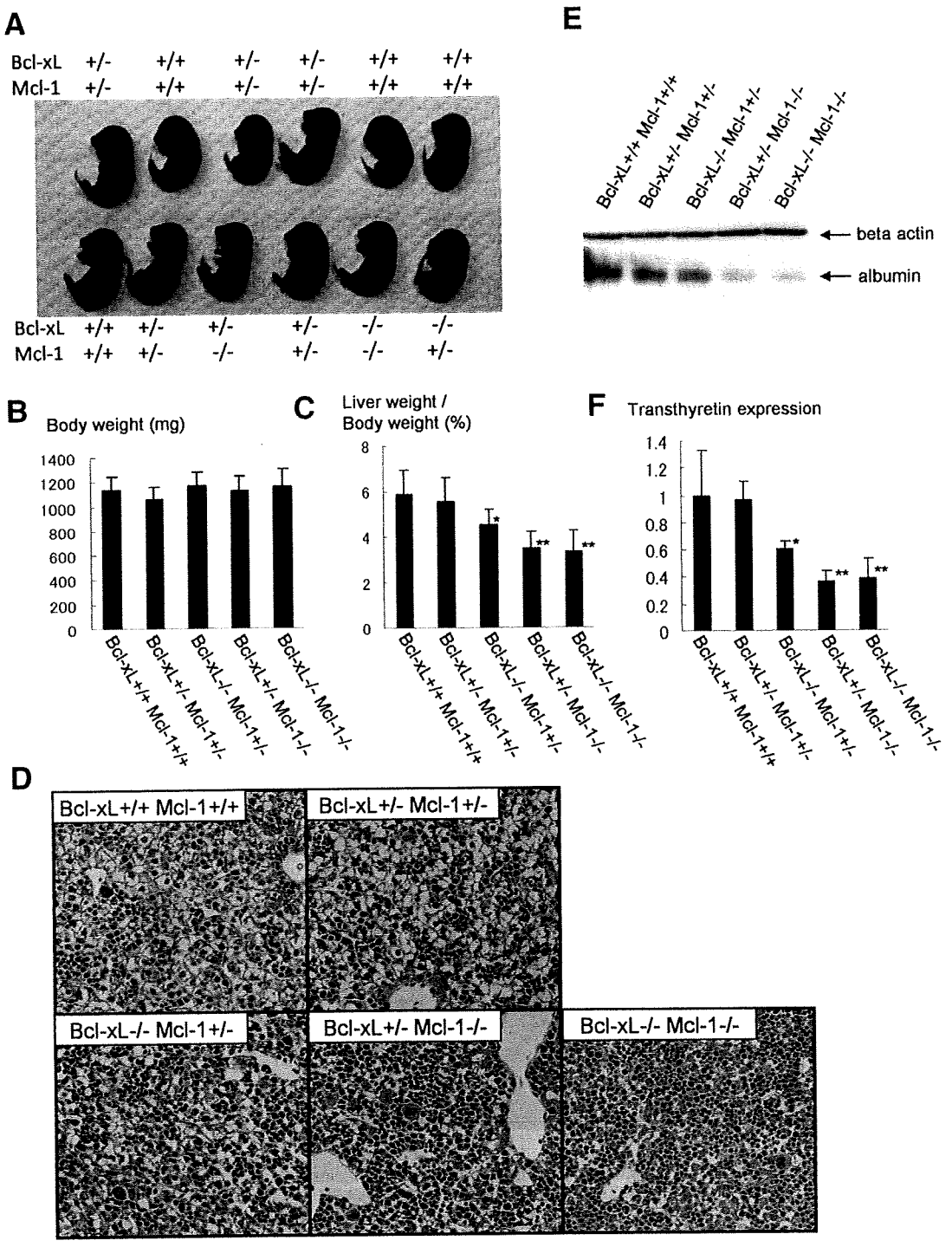

Fig. 4. Hepatocyte-specific Bcl-xL/Mcl-1-deficient embryos. Offspring from mating *bcl-x*$^{flox/+}$ *mcl-1*$^{flox/+}$ *AlbCre* mice and *bcl-x*$^{flox/flox}$ *mcl-1*$^{flox/flox}$ mice were sacrificed on day 18.5 of gestation. Mice were classified into five groups. The *bcl-x*$^{flox/+ \text{ or } flox}$ *mcl-1*$^{flox/+ \text{ or } flox}$ are indicated by Bcl-xL +/+ Mcl-1 +/+; *bcl-x*$^{flox/+}$ *mcl-1*$^{flox/+}$ *AlbCre* are indicated by Bcl-xL +/− Mcl-1 +/−; *bcl-x*$^{flox/flox}$ *mcl-1*$^{flox/+}$ *AlbCre* are indicated by Bcl-xL −/− Mcl-1 +/−; *bcl-x*$^{flox/+}$ *mcl-1*$^{flox/flox}$ *AlbCre* are indicated by Bcl-xL +/− Mcl-1 −/−; *bcl-x*$^{flox/flox}$ *mcl-1*$^{flox/flox}$ *AlbCre* are indicated by Bcl-xL −/− Mcl-1 −/ −. The numbers of embryos analyzed were 30 for Bcl-xL +/+ Mcl-1 +/+, 11 for Bcl-xL +/− Mcl-1 +/−, 8 for Bcl-xL −/− Mcl-1 +/−, 9 for Bcl-xL +/− Mcl-1 −/−, and 10 for Bcl-xL −/− Mcl-1 −/−. (A) Gross appearance of embryos. Representative photo for a litter is shown. (B) Body weight. (C) The ratios of liver weight to body weight. *$P < 0.05$ versus Bcl-xL +/+ Mcl-1 +/+; **$P < 0.05$ versus Bcl-xL +/+ Mcl-1 +/+ and Bcl-xL +/− Mcl-1 +/−. (D) Hematoxylin-eosin staining of the liver sections. (E) Western blot of whole-liver lysate for albumin expression. (F) Real-time RT-PCR analysis for transthyretin expression. The levels were normalized to the group of Bcl-xL +/+ Mcl-1 +/+. *$P < 0.05$ versus Bcl-xL +/+ Mcl-1 +/+; **$P < 0.05$ versus Bcl-xL +/+ Mcl-1 +/+ and Bcl-xL +/− Mcl-1 +/−.

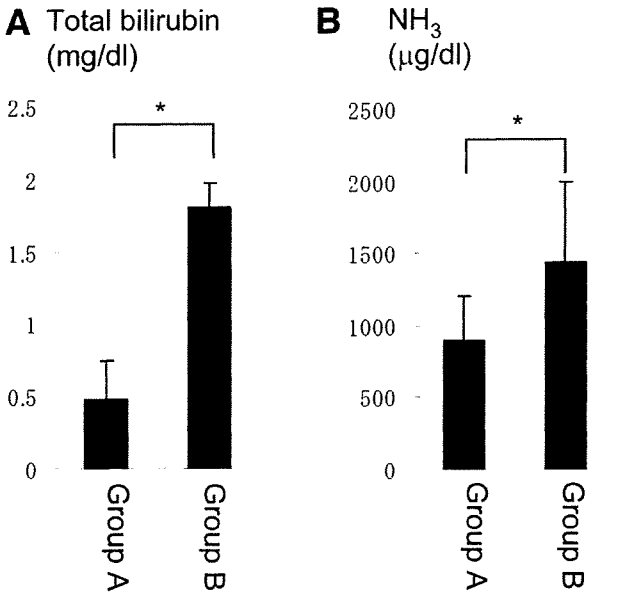

Fig. 5. Plasma biochemistry of hepatocyte-specific Bcl-xL/Mcl-1-deficient neonates 10 hours after birth. Group A (N = 13) was defined as expected survivors including *AlbCre*-negative mice and *bcl-x*$^{flox/+}$ *mcl-1*$^{flox/+}$ *AlbCre* mice. Group B (N = 6) was defined as expected nonsurvivors including *bcl-x*$^{flox/flox}$ *mcl-1*$^{flox/+}$ *AlbCre*, *bcl-x*$^{flox/+}$ *mcl-1*$^{flox/flox}$ *AlbCre*, *bcl-x*$^{flox/flox}$ *mcl-1*$^{flox/flox}$ *AlbCre*. (A) Plasma total bilirubin levels. *$P < 0.05$. (B) Plasma ammonia levels in both groups. *$P < 0.05$.

are in agreement with theirs and further provide evidence that deletion of a single allele for the *mcl-1* gene fails to produce apoptosis phenotypes under physiological conditions, as observed in knockout of the *bcl-x* gene.[13] Mcl-1 heterozygous disrupted mice did not produce apoptosis at least until 16 weeks of age (our unpublished data). It was demonstrated that hepatocyte-specific Mcl-1 knockout mice showed higher levels of liver injury than control mice on anti-Fas antibody injection.[29] However, because mice lacking both *mcl-1* alleles possess preexisting liver injury, it would be difficult to exactly compare liver injury after anti-Fas antibody injection and to conclude whether decreased Mcl-1 expression actually increases the susceptibility to Fas. In the current study, we took advantage of Mcl-1 heterozygous disrupted mice to address this point. They showed significantly higher levels of liver injury after Fas stimulation than wild-type mice, formally proving the significance of Mcl-1 expression under pathological conditions. Furthermore, our data on Mcl-1/Bid–deficient mice implies that the Bid pathway is involved in generating apoptosis found in Mcl-1 knockout mice. Because Bid mediates a variety of cellular stresses in hepatocytes upstream of Mcl-1,[30,31] it will be interesting in future study to determine what stresses generate hepatocyte apoptosis in Mcl-1 knockout mice.

Bcl-xL and Mcl-1 share similar structures and functions.[1] The observations that either deficiency similarly leads to spontaneous hepatocyte apoptosis imply that they play a non-redundant role in maintaining the integrity of hepatocytes in the adult liver. To further understand the relationship of both molecules, we generated hepatocyte-specific Bcl-xL/Mcl-1 knockout mice. Interestingly, mice lacking single alleles for both genes (*bcl-x*$^{+/-}$ *mcl-1*$^{+/-}$) induced spontaneous hepatocyte apoptosis that could not be distinguished from that found in Bcl-xL or Mcl-1 knockout mice. This indicates that, whereas knockout of a single allele of the *bcl-x* or *mcl-1* gene did not produce apoptosis, knockout of two alleles of any combination among both genes was sufficient to produce hepatocyte apoptosis. This finding suggests that both molecules are not independently but rather interdependently required for ensuring integrity of differentiated hepatocytes.

Bcl-xL/Mcl-1-deficient mice as well as mice only having a single allele of either *bcl-x* or *mcl-1* gene displayed a decreased number of hepatocytes and reduced liver size on day 18.5 of gestation and appeared to develop lethal liver failure within 1 day after birth. Because the liver contains a large number of hematopoietic cells during development (Fig. 4D), it is very difficult to determine the expression levels of Bcl-xL or Mcl-1 specifically in hepatocytes in each knockout mouse. Liver development begins on day 8.5 of gestation in the mouse when the liver primordium is delineated from the endoderm.[32] The albumin promoter, which is active in both hepatoblasts and hepatocytes, shows a 20-fold increase in transcriptional activity from day 9.5 to day 12.5 of gestation. The level of albumin then continues to increase as the liver develops simultaneously with the biliary tree and the hepatic bile duct being formed.[33] Thus, the target genes could probably be successfully deleted during embryogenesis in the *AlbCre* recombination system. The observation that Bcl-xL/Mcl-1–deficient mice developed severer phenotypes than Bcl-xL–deficient or Mcl-1–deficient mice supports the idea that Cre-mediated deletion of the target genes actually took place during embryogenesis in our model. In contrast to the knockout of two alleles, knockout of three alleles and more of the *bcl-x* and *mcl-1* genes induced lethal neonatal hepatic failure. Thus, hepatocyte integrity appeared to be strictly controlled by Bcl-xL and Mcl-1 in a gene dose–dependent manner.

Hepatocyte-specific deficiency of both Bcl-xL and Mcl-1 led to significant reduction of liver volume because of impaired hepatocyte development. However, overall, mice with these phenotypes were capable of developing normally until birth and rapidly developed liver failure and died within 1 day after birth. This finding suggests that differentiated hepatocytes are critically required for maintaining host homeostasis after birth but not during embryogenesis. The placenta

plays an important role in nutritional support and detoxification of the embryo. Our data imply that it could probably compensate for most functions of the liver cells during embryogenesis, whereas the liver would turn to the critical organ that is essential for maintaining host homeostasis after birth. Bcl-xL/Mcl-1 knockout mice provide interesting implications for the difference in the impact of differentiated hepatocytes between embryogenesis and the early neonatal period.

In conclusion, Mcl-1 and Bcl-xL are two major Bcl-2 family proteins inhibiting hepatocyte apoptosis. Together with previous work on traditional knockout mice, our data imply that other members, if any, could not compensate for their functions. Mcl-1 and Bcl-xL cooperatively maintain hepatocyte integrity during liver development and in adult liver homeostasis, and their effects are gene-dose dependent. Recent studies also have established that Mcl-1[5-7] and Bcl-xL[18,34] are frequently overexpressed and confer resistance to apoptosis in hepatocellular carcinoma. Therefore, Mcl-1 and Bcl-xL are important apoptosis antagonists in a variety of pathophysiological conditions of the liver.

Acknowledgment: We thank Dr. You-Wen He (Department of Immunology, Duke University Medical Center, Durham, NC) for providing the *mcl-1* floxed mice.

References

1. Youle RJ, Strasser A. The BCL-2 protein family: opposing activities that mediate cell death. Nat Rev Mol Cell Biol 2008;9:47-59.
2. Tsujimoto Y. Cell death regulation by the Bcl-2 protein family in the mitochondria. J Cell Physiol 2003;195:158-167
3. Fischer U, Jänicke RU, Schulze-Osthoff K. Many cuts to ruin: a comprehensive update of caspase substrates. Cell Death Differ 2003;10:76-100.
4. Wei MC, Zong WX, Cheng EH, Lindsten T, Panoutsakopoulou V, Ross AJ, et al. Proapoptotic BAX and BAK: a requisite gateway to mitochondrial dysfunction and death. Science 2001;292:727-730.
5. Sieghart W, Losert D, Strommer S, Cejka D, Schmid K, Rasoul-Rockenschaub S, et al. Mcl-1 overexpression in hepatocellular carcinoma: a potential target for antisense therapy. J Hepatol 2006;44:151-157.
6. Fleischer B, Schulze-Bergkamen H, Schuchmann M, Weber A, Biesterfeld S, Müller M, et al. Mcl-1 is an anti-apoptotic factor for human hepatocellular carcinoma. Int J Oncol 2006;28:25-32.
7 Schulze-Bergkamen H, Fleischer B, Schuchmann M, Weber A, Weinmann A, Krammer PH, et al. Suppression of Mcl-1 via RNA interference sensitizes human hepatocellular carcinoma cells towards apoptosis induction. BMC Cancer 2006;6:232.
8. Llovet JM, Bruix J. Molecular targeted therapies in hepatocellular carcinoma. HEPATOLOGY 2008;48:1312-1327
9. Liu L, Cao Y, Chen C, Zhang X, McNabola A, Wilkie D, et al. Sorafenib blocks the RAF/MEK/ERK pathway, inhibits tumor angiogenesis, and induces tumor cell apoptosis in hepatocellular carcinoma model PLC/PRF/5. Cancer Res 2006;66:11851-11858.
10. Casado M, Mollá B, Roy R, Fernández-Martínez A, Cucarella C, Mayoral R, et al. Protection against Fas-induced liver apoptosis in transgenic mice expressing cyclooxygenase 2 in hepatocytes. HEPATOLOGY 2007;45:631-638.
11. Schulze-Bergkamen H, Brenner D, Krueger A, Suess D, Fas SC, Frey CR, et al. Hepatocyte growth factor induces Mcl-1 in primary human hepatocytes and inhibits CD95-mediated apoptosis via Akt. HEPATOLOGY 2004;39:645-654.
12. Baskin-Bey ES, Huang W, Ishimura N, Isomoto H, Bronk SF, Braley K, et al. Constitutive androstane receptor (CAR) ligand, TCPOBOP, attenuates Fas-induced murine liver injury by altering Bcl-2 proteins. HEPATOLOGY 2006;44:252-262.
13. Takehara T, Tatsumi T, Suzuki T, Rucker EB III, Hennighausen L, Jinushi M, et al. Hepatocyte-specific disruption of Bcl-xL leads to continuous hepatocyte apoptosis and liver fibrotic responses. Gastroenterology 2004;127:1189-1197
14. Dzhagalov I, St John A, He YW. The antiapoptotic protein Mcl-1 is essential for the survival of neutrophils but not macrophages. Blood 2007; 109:1620-1626.
15. Wagner KU, Claudio E, Rucker EB 3rd, Riedlinger G, Broussard C, Schwartzberg PL, et al. Conditional deletion of the Bcl-x gene from erythroid cells results in hemolytic anemia and profound splenomegaly. Development 2000;127:4949-4958.
16. Yin XM, Wang K, Gross A, Zhao Y, Zinkel S, Klocke B, et al. Bid-deficient mice are resistant to Fas-induced hepatocellular apoptosis. Nature 1999; 400:886-891.
17. Takehara T, Hayashi N, Tatsumi T, Kanto T, Mita E, Sasaki Y, et al. Interleukin 1β protects mice from Fas-mediated hepatocyte apoptosis and death. Gastroenterology 1999;117:661-668.
18. Takehara T, Takahashi H. Suppression of Bcl-xL deamidation in human hepatocellular carcinomas. Cancer Res 2003;63:3054-3057.
19. Scaffidi C, Fulda S, Srinivasan A, Friesen C, Li F, Tomaselli KJ, et al. Two CD95 (APO-1/Fas) signaling pathways. EMBO J 1998;17:1675-1687.
20. Faubion WA, Guicciardi ME, Miyoshi H, Bronk SF, Roberts PJ, Svingen PA, et al. Toxic bile salts induce rodent hepatocyte apoptosis via direct activation of Fas. J Clin Invest 1999;103:137-145.
21. Tosh D, Shen CN, Slack JM. Differentiated properties of hepatocytes induced from pancreatic cells. HEPATOLOGY 2002;36:534-543.
22. Veis DJ, Sorenson CM, Shutter JR, Korsmeyer SJ. Bcl-2-deficient mice demonstrate fulminant lymphoid apoptosis, polycystic kidneys, and hypopigmented hair. Cell 1993;75:229-240.
23. Nakayama K, Nakayama K, Negishi I, Kuida K, Sawa H, Loh DY. Targeted disruption of Bcl-2 alpha beta in mice: occurrence of gray hair, polycystic kidney disease, and lymphocytopenia. Proc Natl Acad Sci U S A 1994;91:3700-3704.
24. Print CG, Loveland KL, Gibson L, Meehan T, Stylianou A, Wreford N, et al. Apoptosis regulator bcl-w is essential for spermatogenesis but appears otherwise redundant. Proc Natl Acad Sci U S A 1998;95:12424-12431.
25. Ross AJ, Waymire KG, Moss JE, Parlow AF, Skinner MK, Russell LD, et al. Testicular degeneration in Bclw-deficient mice. Nat Genet 1998;18:251-256.
26. Hamasaki A, Sendo F, Nakayama K, Ishida N, Negishi I, Nakayama K, et al. Accelerated neutrophil apoptosis in mice lacking A1-a, a subtype of the bcl-2-related A1 gene. J Exp Med 1998;188:1985-1992.
27 Motoyama N, Wang F, Roth KA, Sawa H, Nakayama K, Nakayama K, et al. Massive cell death of immature hematopoietic cells and neurons in Bcl-x-deficient mice. Science 1995;267:1506-1510.
28. Rinkenberger JL, Horning S, Klocke B, Roth K, Korsmeyer SJ. Mcl-1 deficiency results in peri-implantation embryonic lethality. Genes Dev 2000;14:23-27.
29. Vick B, Weber A, Urbanik T, Maass T, Teufel A, Krammer PH, et al. Knockout of myeloid cell leukemia-1 induces liver damage and increases apoptosis susceptibility of murine hepatocytes. HEPATOLOGY 2009;49:627-636.
30. Yin XM. Bid, a BH3-only multi-functional molecule, is at the cross road of life and death. Gene 2006;369:7-19.
31. Malhi H, Gores GJ. Cellular and molecular mechanisms of liver injury. Gastroenterology 2008;134:1641-1654.
32. Kaestner KH. The making of the liver: developmental competence in foregut endoderm and induction of the hepatogenic program. Cell Cycle 2005;4:146-1148.
33. Cascio S, Zaret KS. Hepatocyte differentiation initiates during endodermal-mesenchymal interactions prior to liver formation. Development 1991;113:217-225.
34. Takehara T, Liu X, Fujimoto J, Friedman SL, Takahashi H. Expression and role of Bcl-xL in human hepatocellular carcinomas. HEPATOLOGY 2001;34:55-61.

Case report

Two types of drug-resistant hepatitis B viral strains emerging alternately and their susceptibility to combination therapy with entecavir and adefovir

*Nao Kurashige[1], Kazuyoshi Ohkawa[1], Naoki Hiramatsu[1], Isugiko Oze[1], Takayuki Yakushijin[1], Kiyoshi Mochizuki[1], Atsushi Hosui[1], Takuya Miyagi[1], Hisashi Ishida[1], Tomohide Tatsumi[1], Tatsuya Kanto[1], Tetsuo Takehara[1] and Norio Hayashi[1]**

[1]Department of Gastroenterology and Hepatology, Osaka University Graduate School of Medicine, Suita, Osaka, Japan

*Corresponding author: e-mail: hayashin@gh.med.osaka-u.ac.jp

The most serious problem of nucleoside/nucleotide analogue therapy for hepatitis B virus (HBV) infection is the emergence of drug-resistant mutant virus. Here, we describe a patient with chronic hepatitis B infection with a complex drug-resistant mutant virus during sequential therapy with lamivudine (3TC), entecavir (ETV) and adefovir dipivoxil (ADV). The patient was a 52-year-old male with positive hepatitis B e antigen and high HBV DNA (>7.6 $\log_{10}$ copies/ml). Initial 3TC monotherapy offered little benefit and 3TC resistance was established by the virus with rtA181T and not rtM204V/I. HBV DNA was reduced slightly by replacement with ETV monotherapy and was followed by virological breakthrough. At that time, rtA181T was undetectable and the virus with rtM204V and rtL180M became predominant. ETV resistance was established by an additional rtS202G mutation. Efficacy of subsequent combination therapy with ADV and 3TC was limited because of reappearance of the virus with rtA181T, which might confer cross-resistance to 3TC and ADV. Final combination therapy with ETV and ADV reduced HBV DNA to 3.7 $\log_{10}$ copies/ml for 5 months, which was the most effective therapy for this patient. Thus, two kinds of mutant viruses (rtM204V-related and rtA181T-related) appeared alternately in this patient. Combination therapy with ETV and ADV might have been effective because these drugs share therapeutic roles, that is, ETV affects the rtA181T-related virus and ADV affects the rtM204V-related virus. This is the first report suggesting clinical significance of combination therapy with ETV and ADV for controlling replication of the complex drug-resistant mutant HBV.

Introduction

Nucleoside/nucleotide analogues have a better therapeutic effect on chronic hepatitis B virus (HBV) infection than previously used drugs. They strongly suppress HBV replication and retard disease progression [1,2]; however, the most serious problem associated with nucleoside/nucleotide analogues is the emergence of drug-resistant viruses through long-term administration. Drug-resistant viruses for nucleoside/nucleotide analogues occur as a result of amino acid substitutions within the reverse transcriptase (RT) domain of the HBV polymerase gene. Lamivudine (3TC) resistance is primarily caused by mutations rtM204V/I and rtL180M, the latter of which is a compensatory substitution [3,4]. Adefovir dipivoxil (ADV) resistance is associated with the mutations rtA181V/T and/or rtN236T [5]. Entecavir (ETV) resistance is established by substitution(s) at rt184, rt202 and/or rt250 in addition to 3TC-resistant substitutions, rtM204V and rtL180M [6].

Recently, the substitution at rt181 has been reported to confer cross-resistance not only to ADV, but also to other nucleoside/nucleotide analogues [7,8]. Some investigators have suggested that 3TC resistance can occur not only with rtM204V/I, but also with rtA181T [9,10]. A more recent report has shown that rtA181V/T is involved in resistance to multiple drugs, including 3TC, ADV and tenofovir disoproxil fumarate, although the degree of drug resistance varies considerably among HBV strains *in vitro* [8].

In this report, we describe a chronic HBV patient who has a complex drug-resistant mutant virus that was identified during sequential therapy with three nucleoside/nucleotide analogues. In this patient, two kinds of mutant viral strains based on the rtM204V and

rtA181T substitutions appeared alternately. We also refer to the clinical usefulness of combination therapy with ETV and ADV for the mutant HBV strain.

Patient clinical course

The patient was a 52-year-old male who first visited Osaka University Hospital (Osaka, Japan) in September 2004. He had been diagnosed as a chronic HBV carrier 5 years earlier. He was a chronic drinker, with alcohol consumption of approximately 65 g/day. He had also suffered from type-2 diabetes mellitus for >10 years and had undergone insulin therapy for 10 months. The laboratory data at his first visit were alanine aminotransferase (ALT) 68 IU/l (normal level ≤40 IU/l), aspartate aminotransferase (AST) 75 IU/l (normal level ≤40 IU/l), γ-glutamyl transpeptidase (GGT) 189 IU/l (normal level <50 IU/l), fasting plasma glucose (FPG) 239 mg/dl (normal level ≤110 mg/dl), glycated haemoglobin (HbA1c), 10.3% (normal range 4.3–5.8%) and HBV DNA>7.6 $\log_{10}$ copies/ml. Hepatitis B surface antigen (HBsAg) and hepatitis B e antigen (HBeAg) were positive, whereas antibodies against HBsAg (anti-HBs), HBeAg (anti-HBe), hepatitis C virus and HIV were negative. Liver histology showed mild piecemeal necrosis, mild lobular inflammation and mild portal fibrosis; however, steatosis was found in only <5% of the hepatocytes. 3TC (100 mg/day) therapy was commenced in October 2004. Sequencing analysis before therapy revealed no drug-resistance-associated mutations. After starting 3TC therapy, HBV DNA decreased to 6.5 $\log_{10}$ copies/ml in February 2006 and increased again to >7.6 $\log_{10}$ copies/ml in April 2006. ALT levels were almost abnormal and on one occasion flared up to 472 IU/l in December 2005 despite cessation of drinking. rtM204V/I was not detected by repeated PCR-enzyme-linked minisequence assay [11], but rtA181T was found by sequencing analysis in October 2006. At this point, 3TC was switched to ETV monotherapy (0.5 mg/day). The laboratory data at the beginning of ETV administration were ALT 64 IU/l, AST 78 IU/l, GGT 268 IU/l and HBV DNA>7.6 $\log_{10}$ copies/ml. Diabetes mellitus was improved (FPG 123 mg/dl and HbA1c 6.9%) because of a strict diet. During ETV therapy, HBV DNA decreased to 5.6 $\log_{10}$ copies/ml in February 2007, but virological breakthrough was observed in August 2007 (HBV DNA 6.7 $\log_{10}$ copies/ml). As for drug-resistance-associated mutations, rtM204V and rtL180M were detected in September 2007, and rtS202G was detected in January 2008 despite an increasing dose of ETV (1 mg/day). ETV administration was stopped in March 2008 and replaced by combination therapy of 3TC (100 mg/day) with ADV (10 mg/day). The laboratory data at that time were ALT 29 IU/l, AST 49 IU/l, GGT 161 IU/l and HBV DNA 7.0 $\log_{10}$ copies/ml. The combination therapy led to a slight decrease in HBV DNA to 5.6 $\log_{10}$ copies/ml in June 2008. In September 2008, rtA181T was detected again, whereas rtL180M, rtS202G and rtM204V were not detected. From October 2008, a combination therapy with ADV (10 mg/day) and ETV (0.5 mg/day) was carried out. HBV DNA decreased from 5.8 to 3.7 $\log_{10}$ copies/ml for 5 months.

In this patient, ALT fluctuated within the normal to slightly abnormal range (≤60 IU/l) during ETV monotherapy and subsequent combination therapy. Improvement of liver function was observed despite poor control of HBV replication and appeared to be greatly attributed to recovery from alcoholic and diabetes mellitus-related liver diseases. Throughout the follow-up period, no side effects from the nucleoside/nucleotide analogues were observed. The clinical course of the patient is summarized in Figure 1.

Serological and virological assays for HBV

HBsAg, anti-HBs, HBeAg and anti-HBe were determined by chemiluminescent immunoassays. HBV DNA was quantified by a PCR-based method (Amplicor HBV monitor; Roche Diagnostics, Basel, Switzerland). The 3TC-resistant rtM204V/I substitution was examined by PCR-enzyme-linked minisequence assay [11]. Nucleotide sequences of the entire RT region were determined by PCR direct sequencing. The primers BF5 (5′-AAGAGACAGTC ATCCTCAGG-3′, nucleotides 3183–3202) and BR8 (5′-TTGCGTCAGCAAACACTTGG-3′, nucleotides 1195–1176) were used for the amplification. The sequencing analyses were done using sera collected in October 2004, October 2006, September 2007, January 2008 and September 2008 (designated as P1 to P5, respectively; Figure 1).

Results of sequencing analyses

Sequencing data showed that the patient was infected with HBV genotype C according to phylogenetic tree analysis (data not shown). The results of serial sequencing analyses from P1 to P5 are shown in Figure 2. The virus with rtA181T and rtF221Y was detected at P2. By contrast, the virus with rtL180M, rtM204V, rtL229V and rtL269I became predominant at P3. At P4, rtS202G was added, although it occurred incompletely; however, the dominant virus at P5 possessed rtA181T and rtF221Y and was identical to that at P2.

We also compared HBV DNA sequences around rt180 and rt181 obtained at P1–P5 (Figure 3). At P2 and P5, two types of mutations were identified: one was an A670 mutation causing rtA181T and an in-frame stop codon formation at codon 172 of the *S* gene, and

the other was a C669/A670 double mutation, which resulted in rtA181 but avoided the stop codon formation in the *S* gene. At P3 and P4, the A667 mutation, which led to rtL180M, was detected.

Discussion

In this paper, we have described a chronic hepatitis B patient with a complex drug-resistant mutant virus. In this patient, initial 3TC monotherapy offered little benefit and virological breakthrough was observed after administration. 3TC resistance was not caused by rtM204V/I but by rtA181T. After 3TC was replaced by ETV, HBV DNA decreased to 5.6 $\log_{10}$ copies/ml, followed by virological breakthrough for a short period of time. At that time, rtA181T was not detected, and the virus with rtM204V and rtL180M was predominant. This indicates that the virus with rtM204V and rtL180M might have already coexisted as a minor population before ETV therapy, and that the virus with rtA181T might have been reduced because of its susceptibility to ETV. Indeed, the virus with rtA181V/T has been reported to be sensitive to ETV *in vitro* [8]. The ETV resistance-specific rtS202G was not yet seen at the time of virological breakthrough. It was observed a short time later, resulting in the establishment of ETV resistance, although the reasons for virological breakthrough prior to the detection of the ETV-resistant HBV strain remains to be understood.

Subsequently, combination therapy with ADV and 3TC was done because ADV has been reported to have an effect on ETV resistance [12,13]; however, its efficacy was limited and the virus with rtA181T reappeared. The virus with rtM204V, rtL180M and rtS202G became undetectable. This might be because the virus with rtM204V, rtL180M and rtS202G was susceptible

Figure 1. Clinical course of a patient with a complex drug-resistant mutant HBV during sequential therapy with 3TC, ETV and ADV

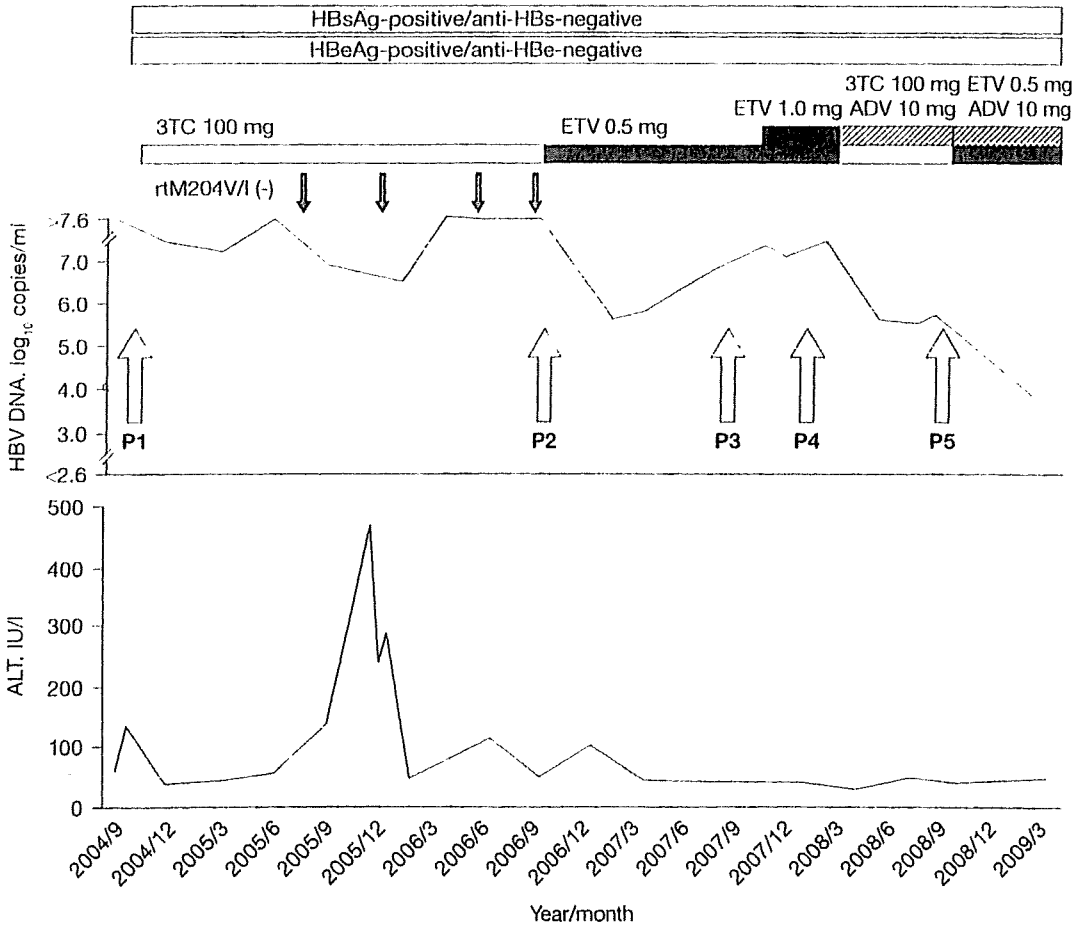

Black arrows represent the absence of the rtM204V/I substitution as detected by PCR-enzyme-linked minisequence assay. White arrows represent the serum sampling points (October 2004, October 2006, September 2007, January 2008 and September 2008 designated as P1 to P5, respectively) for sequencing analysis of the hepatitis B virus (HBV) reverse transcriptase region. ADV, adefovir dipivoxil; ALT, alanine aminotransferase; anti-HBe, antibodies against hepatitis B e antigen; anti-HBs, antibodies against hepatitis B surface antigen; ETV, entecavir; HBeAg, hepatitis B e antigen; HBsAg, hepatitis B surface antigen; 3TC, lamivudine.

Figure 2. Amino acid sequences of the RT region of the HBV polymerase gene at serum sampling points P1–P5

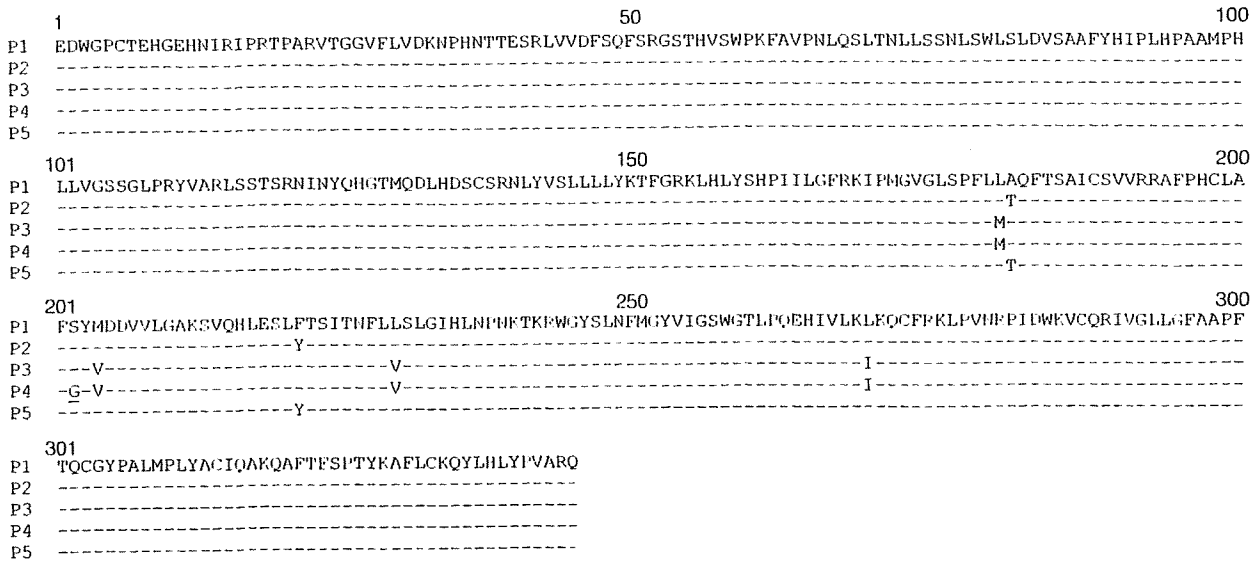

An amino acid residue identical to that of the top sequence is shown by dashes. The underlined residue indicates the coexistence with the identical residue to the top sequence. Sampling points were at October 2004, October 2006, September 2007, January 2008 and September 2008 (designated as P1 to P5, respectively). HBV, hepatitis B virus; RT, reverse transcriptase

Figure 3. DNA and amino acid sequences around the positions rt180 and rt181 at serum sampling points P1–P5

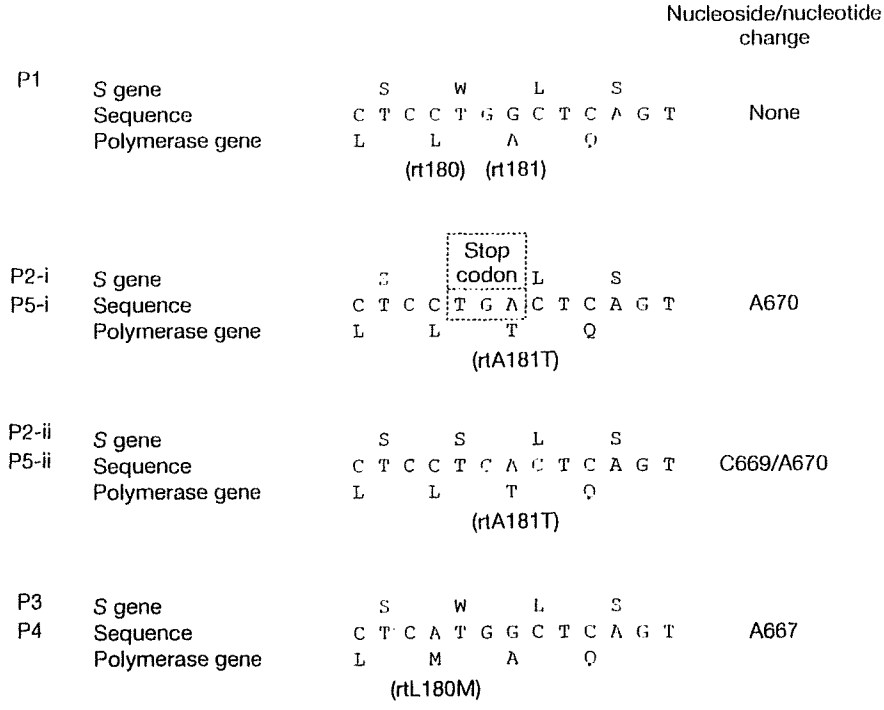

Mutated nucleosides/nucleotides and substituted amino acid residues are underlined. As for nucleoside/nucleotide changes, the nucleoside/nucleotide numbering is according to the representative hepatitis B virus (HBV) genotype C strain (GenBank accession number AB033550) [15], where position 1 is an *EcoRI* recognition site. Sampling points were at October 2004, October 2006, September 2007, January 2008 and September 2008 (designated as P1 to P5, respectively).

to ADV, whereas the virus with rtA181T revealed resistance to 3TC and possibly ADV. Final combination therapy with ETV and ADV resulted in a decrease in HBV DNA to 3.7 $\log_{10}$ copies/ml for 5 months, which was the most effective therapeutic regimen for this patient. Thus, two kinds of drug-resistant viral strains, the rtA181T-related strain and the rtM204V-related strain, appeared alternately in this patient. It is noteworthy that combination therapy with ETV and ADV was effective against such a complex mutant HBV. This might be because of the sharing of therapeutic roles of these drugs: ETV for the rtA181T-related strain and ADV for the rtM204V-related strain.

rtA181T, which is generally caused by the A670 mutation, results in the in-frame stop codon formation at codon 172 of the *S* gene. In this patient, the virus with the C669/A670 double mutation, which could produce the surface protein, coexisted with the virus with the A670 mutation alone. A similar virus with the T669/A670 double mutation, which compensates for the defect of surface protein production, has also been reported [7,14].

In summary, we have reported on a complex drug-resistant mutant HBV related to both rtA181T and rtM204V substitutions in a patient with chronic HBV, who received sequential therapy of nucleoside/nucleotide analogues. We also showed for the first time that combination therapy with ETV and ADV might be of clinical significance for controlling replication of complex mutant HBV.

Disclosure statement

The authors declare no competing interests.

References

1. Lavanchy D. Hepatitis B virus epidemiology, disease burden, treatment, and current and emerging prevention and control measures. *J Viral Hepat* 2004; 11:97–107.
2. Keeffe EB, Dieterich DT, Han SHB, *et al.* A treatment algorithm for the management of chronic hepatitis B virus infection in the United States: 2008 update. *Clin Gastroenterol Hepatol* 2008; 6:1315–1341.
3. Allen MI, Deslauriers M, Andrews CW, *et al.* Identification and characterization of mutations in hepatitis B virus resistant to lamivudine. *Hepatology* 1998; 27:1670–1677.
4. Liaw YF, Chien RN, Yeh CT, Tsai SL, Chu CM. Acute exacerbation and hepatitis B virus clearance after emergence of YMDD motif mutation during lamivudine therapy. *Hepatology* 1999; 30:567–572.
5. Hadziyannis SJ, Tassopoulos NC, Heathcote EJ, *et al.* Long-term therapy with adefovir dipivoxil for HBeAg-negative chronic hepatitis B for up to 5 years. *Gastroenterology* 2006; 131:1743–1751.
6. Tenney DJ, Rose RE, Baldick CJ, *et al.* Two-year assessment of entecavir resistance in lamivudine-refractory hepatitis B virus patients reveals different clinical outcomes depending on the resistance substitutions present. *Antimicrob Agents Chemother* 2007; 51:902–911.
7. Yatsuji H, Noguchi C, Hiraga N, *et al.* Emergence of a novel lamivudine-resistant hepatitis B virus variant with a substitution outside the YMDD motif. *Antimicrob Agents Chemother* 2006; 50:3867–3874.
8. Villet S, Pichoud C, Billioud G, *et al.* Impact of hepatitis B virus rtA181V/T mutants on hepatitis B treatment failure. *J Hepatol* 2008; 48:747–755.
9. Yeh CT, Chien RN, Chu CM, *et al.* Clearance of the original hepatitis B virus YMDD-motif mutants with emergence of distinct lamivudine-resistant mutants during prolonged lamivudine therapy. *Hepatology* 2000; 31:1318–1326.
10. Pai SB, Bozdayi AM, Pai RB, *et al.* Emergence of a novel mutation in the FLLA region of hepatitis B virus during lamivudine therapy. *Antimicrob Agents Chemother* 2005; 49:2618–2624.
11. Kobayashi S, Ide T, Sata M. Detection of YMDD motif mutations in some lamivudine-untreated asymptomatic hepatitis B virus carriers. *J Hepatol* 2001; 34:584–586.
12. Villet S, Ollivet A, Pichoud C, *et al.* Stepwise process for the development of entecavir resistance in a chronic hepatitis B virus infected patient. *J Hepatol* 2007; 46:531–538.
13. Yatsuji H, Hiraga N, Mori N, *et al.* Successful treatment of an entecavir-resistant hepatitis B virus variant. *J Med Virol* 2007; 79:1811–1817.
14. Yatsuji H, Suzuki F, Sezaki H, *et al.* Low risk of adefovir resistance in lamivudine-resistant chronic hepatitis B patients treated with adefovir plus lamivudine combination therapy: two-year follow-up. *J Hepatol* 2008; 48:923–931.
15. Okamoto H, Tsuda F, Sakugawa H, *et al.* Typing hepatitis B virus by homology in nucleotide sequence: comparison of surface antigen subtypes. *J Gen Virol* 1988; 69:2575–2583.

Accepted for publication 24 May 2009

Anticancer Chemotherapy Inhibits MHC Class I–Related Chain A Ectodomain Shedding by Downregulating ADAM10 Expression in Hepatocellular Carcinoma

Keisuke Kohga, Tetsuo Takehara, Tomohide Tatsumi, Takuya Miyagi, Hisashi Ishida, Kazuyoshi Ohkawa, Tatsuya Kanto, Naoki Hiramatsu, and Norio Hayashi

Department of Gastroenterology and Hepatology, Osaka University Graduate School of Medicine, Osaka, Japan

Abstract

MHC class I–related chain A (MICA) is a ligand for the NKG2D-activating immunoreceptor that mediates activation of natural killer (NK) cells. The ectodomain of MICA is shed from tumor cells, which may be an important means of evading antitumor immunity. We previously reported that patients with hepatocellular carcinoma (HCC) display high levels of soluble MICA in circulation, which could be downregulated by chemotherapy. The present study shows that anti-HCC drugs suppress MICA ectodomain shedding by inhibiting expression of a disintegrin and metalloproteinase 10 (ADAM10). Both ADAM10 and CD44, a typical substrate of the ADAM10 protease, were expressed in human HCC tissues and HCC cells but not in normal liver tissues or cultured hepatocytes. Small interfering RNA–mediated knockdown experiments revealed that ADAM10 is a critical sheddase for both MICA and CD44 in HCC cells. Of interest is the finding that epirubicin clearly downregulated ADAM10 expression and MICA shedding in HCC cells; its suppressive effect on MICA shedding was abolished in ADAM10-depleted cells. Epirubicin treatment also enhanced the NKG2D-mediated NK sensitivity of HCC cells. Patients with HCC had significantly higher levels of serum-soluble CD44, which correlated well with serum-soluble MICA levels, thus suggesting a close link between ADAM10 activity and MICA shedding in these patients. Soluble MICA and CD44 levels were downregulated with a significant correlation in patients treated by transarterial chemoembolization using epirubicin. In conclusion, anticancer drugs can modulate expression of ADAM10, which is critically involved in MICA ectodomain shedding. Epirubicin therapy may have a previously unrecognized effect on antitumor immunity in HCC patients. [Cancer Res 2009;69(20):8050–7]

Introduction

Hepatocellular carcinoma (HCC) is one of the leading causes of cancer deaths worldwide. Chronic liver disease caused by hepatitis virus infection and nonalcoholic steatohepatitis leads to a predisposition for HCC, with liver cirrhosis, in particular, being considered a premalignant condition (1, 2). With regard to treatment, surgical resection or percutaneous techniques such as ethanol injection and radiofrequency ablation are considered to be choices for curable treatment of localized HCC, whereas transcatheter arterial chemoembolization (TACE) is a well-established technique for more advanced HCC (3). The liver contains a large compartment of innate immune cells [natural killer (NK) cells and natural killer T cells] and acquired immune cells (T cells; refs. 4, 5), but the activation of these immune cells after HCC treatments remains unclear. If such treatments can efficiently activate abundant immune cells in the liver, this could lead to the establishment of attractive new strategies for HCC treatment.

MHC class I–related chain A and B (MICA and MICB) are ligands for NKG2D expressed on a variety of immune cells (6). In contrast to classic MHC class I molecules, MICA/B are rarely expressed on normal cells but frequently on tumor cells (7–10). The engagement of MICA/B and NKG2D strongly activates NK cells and costimulates T cells, enhancing their cytolytic activity and cytokine production (11). Thus, the MICA/B-NKG2D pathway is an important mechanism by which the host immune system recognizes and kills transformed cells (12). In addition to those membrane-bound forms, MICA/B molecules are also cleaved proteolytically from tumor cells and appear as soluble forms in sera of patients with malignancy (13–15). Soluble MICA/B in circulation downregulates NKG2D expression and disturbs NKG2D-mediated antitumor immunity (9, 10, 13). We previously reported that soluble MICA could be detected in sera of HCC patients (16) and that TACE treatment reduces the levels of soluble MICA and thereby upregulates the expression of NKG2D (17). Thus, cancer therapy may have a beneficial effect on NKG2D-mediated immune responses.

The release of soluble MICA/B from tumor cells is impaired by metalloproteinase inhibitors, suggesting the involvement of members of the metzincin superfamily, such as ADAM proteins (14, 18). In addition, ERp5, related to protein disulfide isomerase, is required for the MICA shedding as it reduces disulfide bond of the α3 domain of MICA (19). Although it may not be a direct protease for MICA, it may enable proteolytic cleavage through conformational change. Recently, it was reported that MICA shedding of 293T fibroblast cells and HeLa cervical cancer cells was inhibited by silencing of the ADAM10 and ADAM17 proteases (20). This suggests that ADAM family proteins may be a therapeutic target for enhancing antitumor immunity, but how to therapeutically modulate these proteins is still not clear. Furthermore, it remains to be determined whether ADAMs can regulate MICA shedding in a clinical setting.

In the present study, we showed that ADAM10, but not ADAM17, was critically required for MICA shedding in human HCC cells. Of importance is the discovery that epirubicin, a widely used anti-HCC drug, was capable of downregulating ADAM10 expression and

---

Note: Supplementary data for this article are available at Cancer Research Online (http://cancerres.aacrjournals.org/).

K. Kohga, T. Takehara, and T. Tatsumi contributed equally to this work.

Requests for reprints: Norio Hayashi, Department of Gastroenterology and Hepatology, Osaka University Graduate School of Medicine, 2-2 Yamadaoka, Suita, Osaka 565-0871, Japan. Phone: 81-6-6879-3621; Fax: 81-6-6879-3629; E-mail: hayashin@gh.med.osaka-u.ac.jp.

doi:10.1158/0008-5472.CAN-09-0789

activity in HCC cells; it can thus inhibit MICA shedding and enhance NK sensitivity. ADAM10 was immunohistochemically detected in HCC tissues and a correlation was observed between soluble MICA levels and ADAM10 activity determined by soluble CD44 levels in HCC patients. The present study sheds light on previously unrecognized effects of an anticancer drug on modulating ADAM family proteins and MICA shedding and thus suggests a promising aspect for chemoimmunotherapy against human HCC.

Materials and Methods

Liver tissues and immunohistochemistry. Human HCC tissues (n = 8) and normal liver tissues (n = 2) obtained at surgical resection were used. Informed consent, under an institutional review board–approved protocol,

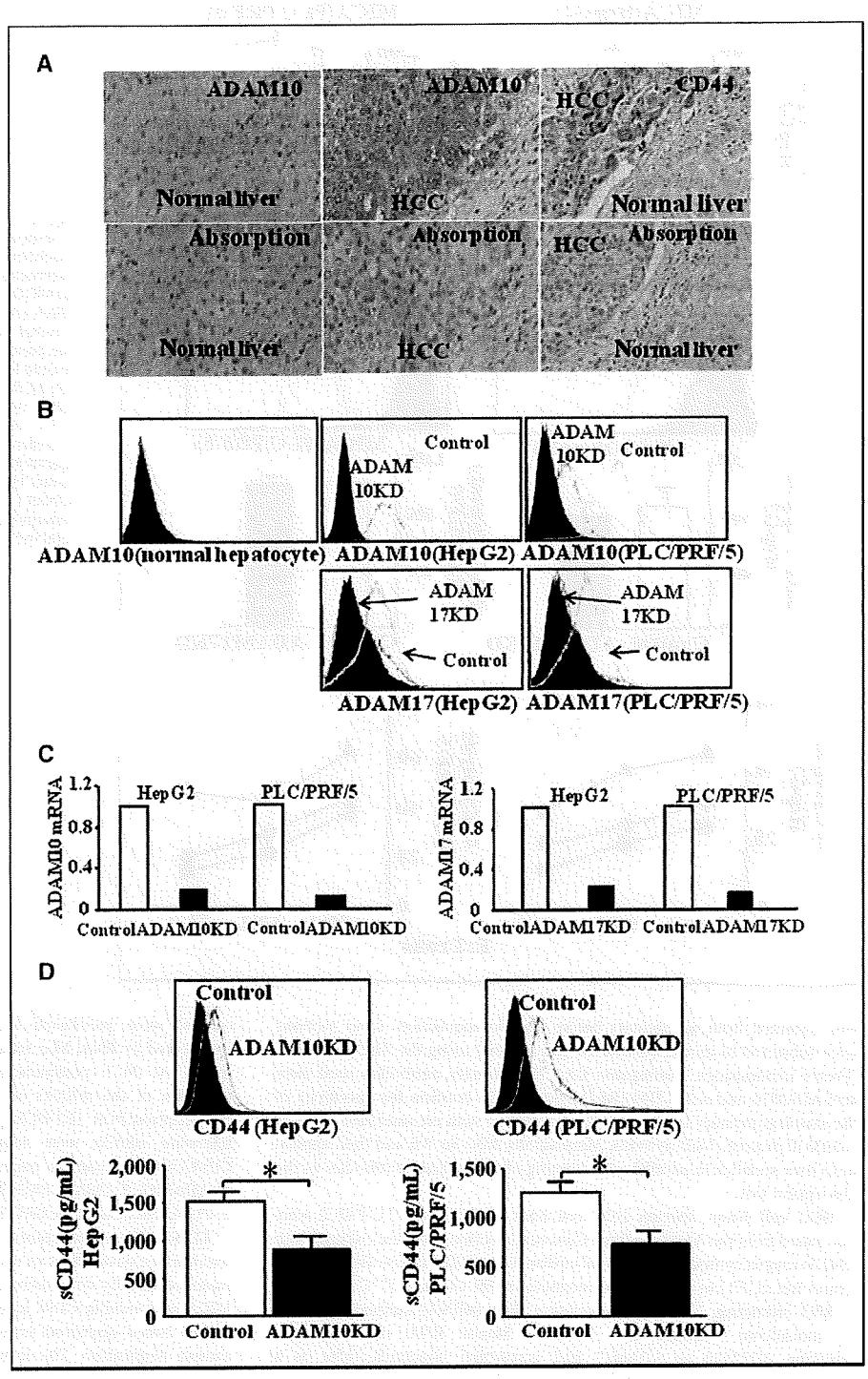

Figure 1. Expression of ADAM10 and CD44 in human HCC tissues and ADAM10 or ADAM17 knockdown in human HCC cells. *A*, immunohistochemical detection of ADAM10 and CD44 in human HCC tissues (n = 8) and normal liver tissues (n = 2). Liver sections were stained with the corresponding antibodies (*top panels*). Both primary antibodies were incubated with recombinant CD44 and ADAM10 proteins and then applied to liver sections in parallel as the absorption test (*bottom panels*). Representative images are shown. *B* and *C*, expression of ADAM10 or ADAM17 in human primary hepatocyte and HCC cell lines (*HepG2* and *PLC/PRF/5*). Cells were treated with ADAM10 siRNA, ADAM17 siRNA, or control siRNA, and subjected to analysis of ADAM10 or ADAM17 expression by flow cytometry (*B*) or real-time RT-PCR (*C*). *Histograms*, anti-ADAM10 or anti-ADAM17 staining of ADAM10 or ADAM17 siRNA-treated cells (*ADAM10KD* or *ADAM17KD*, *black dotted line*) and control siRNA-treated cells (*Control*, *gray line*), respectively. *Closed histograms*, control IgG staining. *D*, the expression of membrane-bound CD44 on HCC cells treated with ADAM10 siRNA (ADAM10KD, *black line*) or control siRNA (*Control*, *gray line*) was evaluated by flow cytometry (*top panels*). *Closed histograms*, control IgG staining. Soluble CD44 (*sCD44*) production from HCC cells treated with ADAM10 siRNA or control siRNA were evaluated by specific ELISA (*bottom panels*). *, $P < 0.05$.

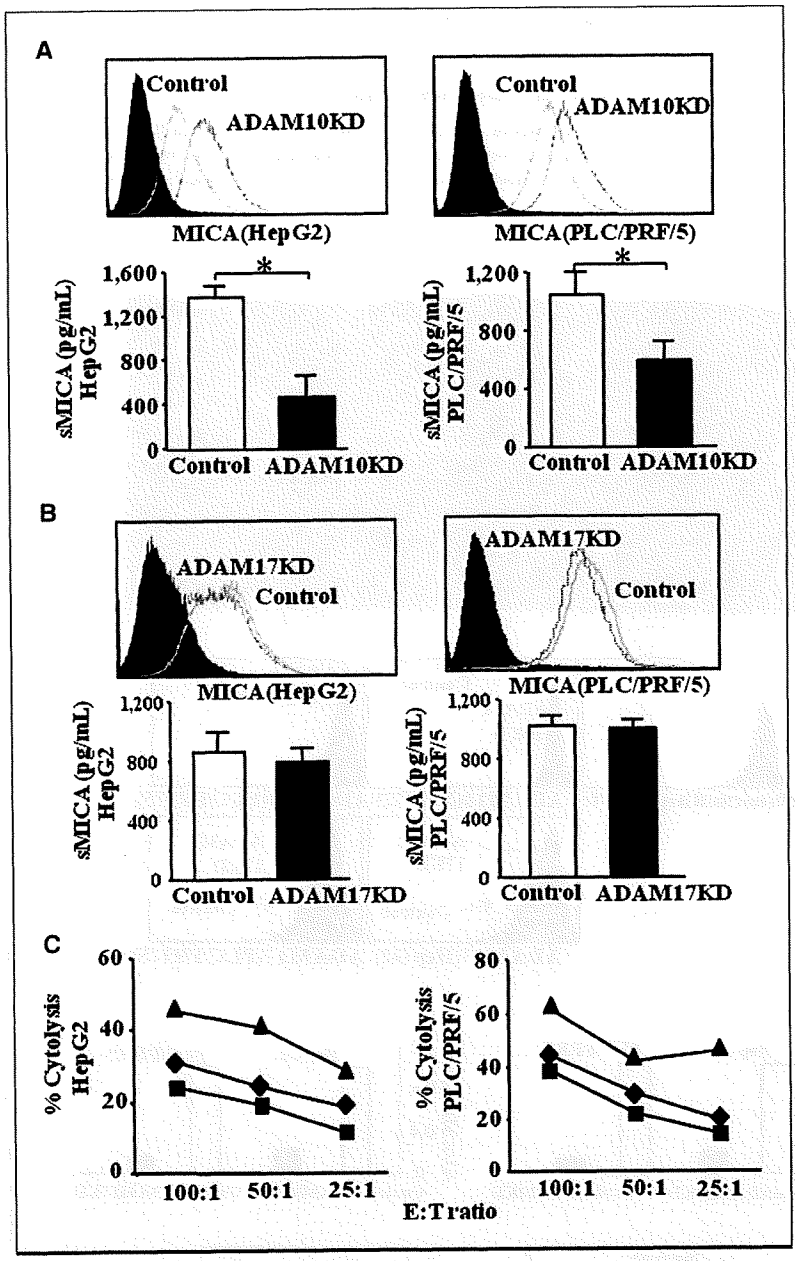

Figure 2. Expression of MICA in ADAM10 or ADAM17 knockdown HCC cells and NK sensitivity in ADAM10 knockdown HCC cells. *A* and *B*, the expression of membrane-bound MICA on HCC cells treated with ADAM10 siRNA (*ADAM10KD, black line*; *A*), ADAM17 siRNA (*ADAM17KD, black line*; *B*), or control siRNA (*Control, gray line*) was evaluated by flow cytometry (*top panels*). *Closed histograms*, control IgG staining. Soluble MICA (*sMICA*) production from HCC cells treated with ADAM10 siRNA (*A*), ADAM17 siRNA (*B*), or control siRNA were evaluated by specific ELISA (*bottom panels*). *, $P < 0.05$. *C*, HCC cells treated with ADAM10 siRNA or control siRNA were subjected to ^{51}Cr-release assay against NK cells. Cytolytic activity of NK cells against control HCC cells (■) or ADAM10 knockdown HCC cells without (▲) or with blocking antibody of MICA/B (6D4; ♦). Representative results are shown. Similar results were obtained from three independent experiments.

was obtained from all patients before sample acquisition. Liver sections were subjected to immunohistochemical staining using the ABC procedure (Vector Laboratories, Burlingame, CA). The primary antibodies used were anti-ADAM10 and anti-CD44 (R&D Systems). To confirm the specificity of the staining, primary antibodies were incubated with recombinant CD44 or ADAM10 protein (R&D Systems, Minneapolis, MN) for 3 h and then applied onto liver sections in parallel with staining of the primary antibodies as the absorption test.

HCC cell lines. Human HCC cell lines HepG2 and PLC/PRF/5 were purchased from the American Type Culture Collection and were cultured with DMEM supplemented with 10% fetal bovine serum (GIBCO/Life Technologies, Grand Island, NY) in a humidified incubator at 5% CO_2 and 37°C.

RNA silencing. The small interfering RNA (siRNA) method was used to knockdown ADAM10 and ADAM17. Stealth RNAi oligonucleotide targeting ADAM10 or ADAM17 and scrambled oligonucleotides as a control were purchased from Invitrogen (Carlsbad, CA). Cells were transfected by RNAi Max transfection reagent (Invitrogen) with 50 nmol/L siRNA. At 24 h posttransfection, the cells were analyzed for specific depletion of the mRNAs of ADAM10 and ADAM17 by real-time reverse transcription-PCR (RT-PCR; Applied Biosystems, Foster City, CA). The following siRNAs were used: ADAM10, 5′-AUAUCUGGGCAAUCACAG-CUUCUCG-3′; scramble control, 5′-AUACUUGGUCAACGCACUUCGAUGG-3′; ADAM17, 5′-UGAACAAGCUCUUCAGGUGGUUCUC-3′; scramble control, 5′-UGAUUAGAACUCUCGACUGGUGCUC-3′.

ELISA. The supernatants of cultured cells were harvested at 24 h after transfection with siRNA as well as sera from HCC patients ($n = 97$) and age-matched healthy volunteers ($n = 32$) were subjected to analysis of soluble MICA and soluble CD44 levels. Informed consent, under an institutional review board–approved protocol, was obtained from all patients before sample acquisition. The levels of soluble MICA and soluble CD44 were

determined by DuoSet MICA eELISA kit (R&D Systems) and soluble CD44std ELISA (Abcam, Cambridge, MA), respectively.

Flow cytometry. For the detection of membrane-bound MICA and CD44, cells were incubated with an anti-MICA–specific antibody (2C10, Santa Cruz Biotechnology, Santa Cruz, CA) or anti-CD44 antibody (R&D Systems) and stained with phycoerythrin (PE)-goat anti-mouse immunoglobulin (Beckman Coulter) as a secondary reagent and then subjected to flow cytometric analysis. For the detection of ADAM10 or ADAM17, cells were fixed and permeabilized with Cytofix/Cytoperm (BD Biosciences, San Jose, CA) and stained with PE-conjugated anti-ADAM10 or anti-ADAM17 antibody (R&D Systems). Flow cytometric analysis was performed using a FACScan flow cytometer (Becton Dickinson).

Plasmid construction of pMyc-MICA. MICA full coding cDNA was isolated from Huh7, human HCC cells, using a conventional RT-PCR method (Supplementary Fig. S1, DDBJ/EMBL/Genbank accession number AB506764) and inserted into the *Hin*dIII-*Xba*I site of pcDNA3 (Invitrogen). A C-myc tag was placed between the leader peptide and the α1 domain of MICA by site-specific mutagenesis using a QuikChange site-directed mutagenesis kit (Stratagene, La Jolla, CA) referred to as pMyc-MICA. Cells were transfected with pMyc-MICA using a Lipofectamine LTX reagent (Invitrogen). The green fluorescent protein (GFP)–expressing vector (pEGFP-C1, Clontech, Mountain View, CA) was cotransfected to evaluate the transfection efficiency.

Immunoprecipitation. Cells or tissues were homogenized in lysis buffer containing 1% NP40, 0.5% sodium deoxycholate, 0.1% SDS, 50 μg/mL aprotinin, 100 μg/mL phenylmethylsulfonyl fluoride, 1 mmol/L sodium orthovanadate, 50 mmol/L sodium fluoride, and PBS. To the cell supernatants, 0.5% NP40 and a cocktail of protease inhibitors were added. The protein contents of the samples were determined by BCA protein assay kit (Pierce, Rackford, IL). Immunoprecipitation with anti–c-Myc beads was performed for 1 h at 4°C. Immunocomplexes were eluted by a c-Myc–tagged peptide solution (MBL, Woburn, MA). The samples after immunoprecipitation were treated with 250 mU of N-glycosidase F (Roche, Mannheim, Germany) for 3 h at 37°C.

Western blotting. The total cellular protein was electrophoretically separated using SDS-12% polyacrylamide gels and transferred onto polyvinylidene difluoride membrane. The membrane was blocked in TBS-Tween containing 5% skim milk for 1 h and then probed with anti-Myc mouse monoclonal antibody (Cell Signaling Technology, Danvers, MA) at 4°C overnight. Horseradish peroxidase–conjugated anti-rabbit antibody and SuperSignal West Pico System (Pierce) were used for the detection of blots.

Real-time RT-PCR. Total RNA was isolated using RNeasy Mini Kit (Qiagen K.K., Tokyo, Japan) and was reverse transcribed using SuperScript III First-Strand Synthesis System (Invitrogen). The mRNA levels were evaluated using ABI PRISM 7900 Sequence Detection System (Applied Biosystems). Ready-to-use assays (Applied Biosystems) were used for the quantification of ADAM10 (Hs00153853_m1), ADAM17 (Hs00234221_m1), MICA (Hs00792195_m1), β-actin (Hs99999903_m1), and CD44 (Hs00174139_m1) mRNAs according to the manufacturer's instructions. The thermal cycling conditions for all genes were 2 min at 50°C and 10 min at 95°C, followed by 40 cycles at 95°C for 15 s and 60°C for 1 min. β-Actin mRNA from each sample was quantified as an endogenous control of internal RNA.

WST-8 assay. HepG2 and PLC/PRF/5 cells were treated with different concentrations of epirubicin for 24 h. Cell growth of epirubicin-treated HCC cells was determined by WST-8 assay (Nacalai Tesque, Kyoto, Japan) as previously described (21).

NK cell analysis. NK cells were isolated from human peripheral blood mononuclear cells by magnetic cell sorting using CD56 MicroBeads (Miltenyl Biotech, Auburn, CA) as previously described (16). The cytolytic ability of NK cells was assessed by 4-h ^{51}Cr-releasing assay with or without MICA/B-blocking antibody (6D4; ref. 7), which binds to the α1 and α2 domains of MICA and MICB. 6D4 was a generous gift from Drs. Veronika Groh and Thomas Spies (Fred Hutchinson Cancer Research Center, Seattle, WA).

Statistics. All values were expressed as the mean and SD. The statistical significance of differences between the groups was determined by applying Student's *t* test or two-sample *t* test with Welch correction after each group

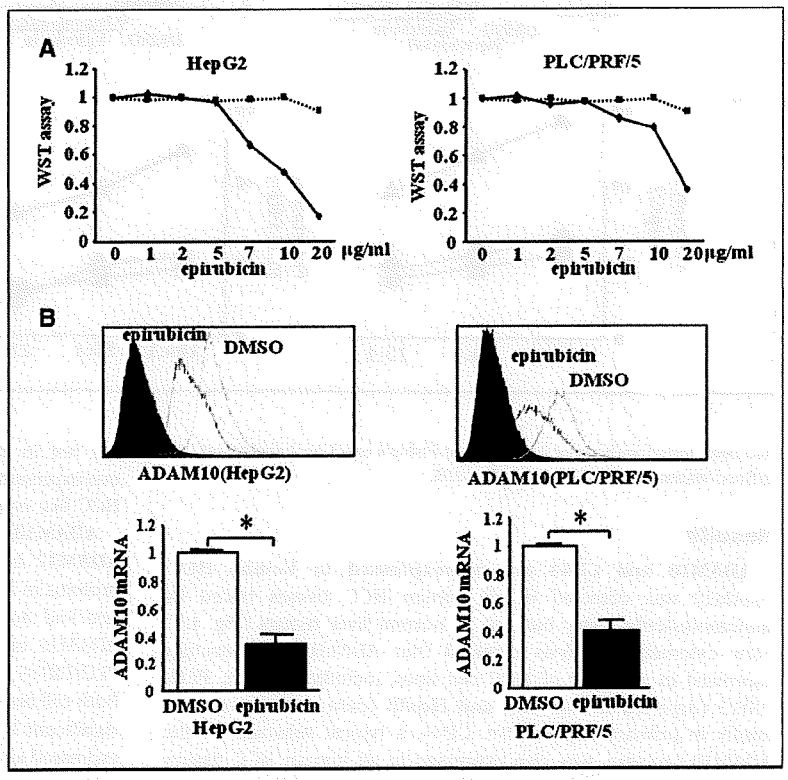

Figure 3. Expression of ADAM10 in epirubicin-treated HCC cells. *A*, the cytotoxicity of epirubicin to human HCC cells was evaluated by WST-8 assay. Cells were treated with different doses of epirubicin (*solid lines*) or vehicle (*DMSO*; *dotted lines*) for 24 h, and the viability of the cells was evaluated by the WST-8 assay. *B*, ADAM10 expression of epirubicin-treated HCC cells. Cells were treated with a nontoxic dose of 1 μg/mL epirubicin (*black lines*) or vehicle (DMSO, *gray lines*) for 24 h and their ADAM10 expression was evaluated by flow cytometry (*top panels*). *Closed histograms*, control IgG staining. Total RNA was extracted at 24 h of epirubicin treatment and mRNA levels of ADAM10 were evaluated by real-time RT-PCR (*bottom panels*). *, $P < 0.05$.

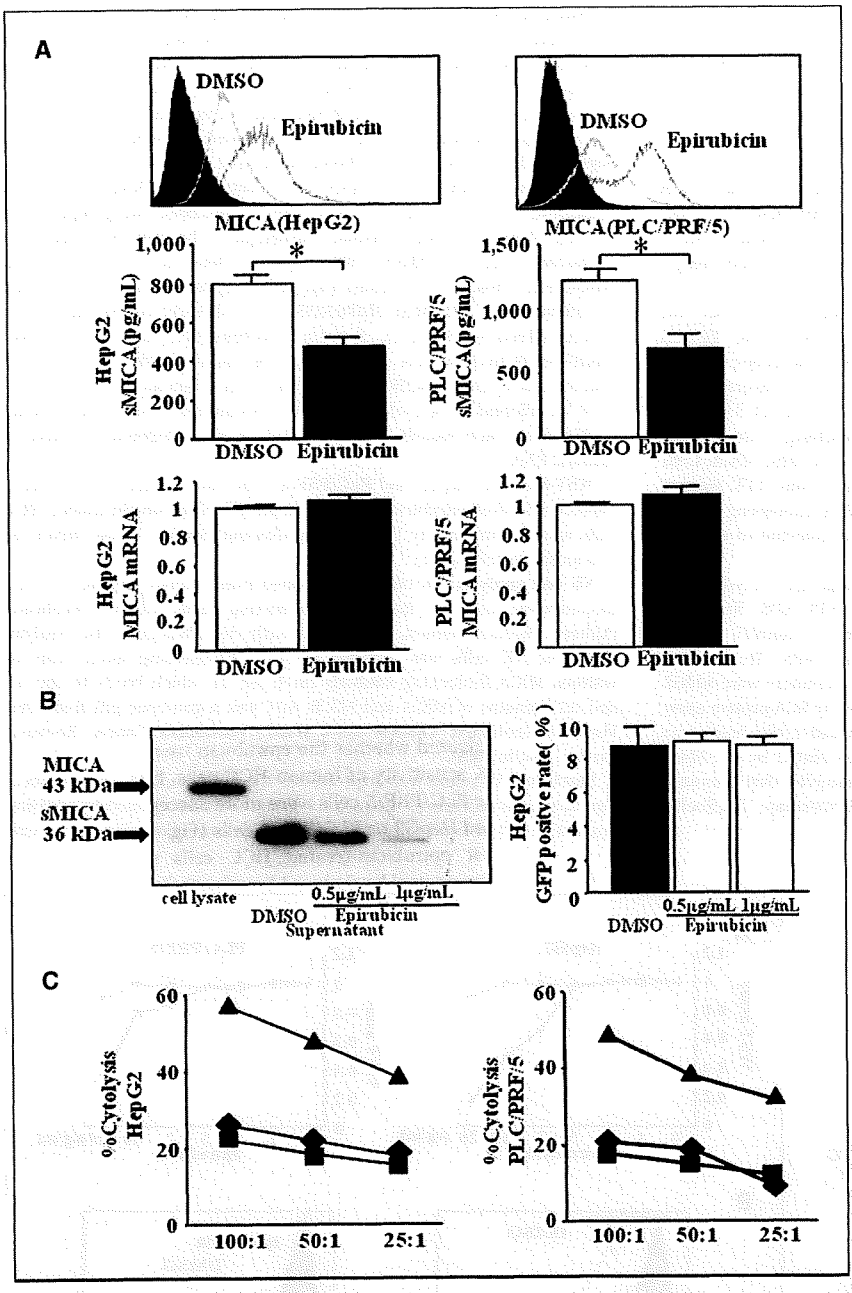

Figure 4. Expression and shedding of MICA in epirubicin-treated HCC cells. *A*, HCC cells were treated with a nontoxic dose of 1 μg/mL epirubicin (*black lines*) or vehicle (DMSO, *gray lines*) for 24 h and their expression of membrane-bound MICA and MICA mRNA was evaluated by flow cytometry (*top panels*) and real-time RT-PCR (*bottom panels*), respectively. *Closed histograms*, control IgG staining in flow cytometry. At the same time, 24-h culture supernatants were subjected to the analysis of soluble MICA (*sMICA*) levels by ELISA (*middle panels*). *, $P < 0.05$. *B*, HepG2 cells were transfected with pMyc-MICA and pEGFP-C1, cultured with 0.5 to 1 μg/mL epirubicin or vehicle (DMSO) for 24 h. Cell lysates from HepG2 cells and 24-h culture supernatants of epirubicin- or vehicle-treated HepG2 cells were immunoprecipitated with anti-Myc. The resulting immunoprecipitates were eluted, treated with N-glycanase, and subjected to Western blot analysis for MICA (*left*). Transfection efficacies were equal in all treatment groups as evidenced by similar GFP-positive cell rates (*right*). *C*, the cytolytic activity of NK cells against HCC cells. Vehicle-treated cells (■) or epirubicin-treated cells without (▲) or with blocking antibody of MICA/B (6D4; ♦) were subjected to ^{51}Cr-release assay. Representative results are shown. Similar results were obtained from three independent experiments.

had been tested with equal variance and Fisher's exact probability test. We defined statistical significance as $P < 0.05$.

Results

ADAM10 and CD44 are overexpressed in human HCC. ADAM10 was detected in all human HCC tissues tested by immunohistochemistry but not in normal liver tissues (Fig. 1*A*). Flow cytometric analysis revealed that ADAM10 was strongly expressed in a variety of HCC cell lines, including HepG2, PLC/PRF/5 (depicted in Fig. 1*B*), and Hep3B (data not shown), but faintly in primary hepatocytes. CD44, a typical substrate of the ADAM10 protease, was also expressed in all human HCC tissues but not in normal liver tissues (Fig. 1*A*). The data suggest that overexpression of ADAM10 and CD44 is a characteristic of human HCC like other malignancies (22).

ADAM10 is involved in MICA shedding of HCC cells but ADAM17 is not. To examine the involvement of ADAM family proteins in MICA ectodomain shedding, ADAM10 or ADAM17 were knocked down in HCC cells using a siRNA-mediated procedure. ADAM10 expression was clearly suppressed in HepG2 cells and PLC/PRF/5 cells at both mRNA and protein levels (Fig. 1*B* and *C*). Both cell lines expressed CD44 on the cellular surface and produced significant levels of soluble CD44 (Fig. 1*D*), indicating that CD44 is expressed and shed from those cell lines. ADAM10 knockdown (KD)

led to an increase in CD44 expression on HCC cells and a decrease in soluble CD44 levels in culture supernatants (Fig. 1*D*). Because ADAM10 has been established as being a sheddase for CD44, siRNA-mediated knockdown of ADAM10 suppressed not only the expression but also the activity of ADAM10 in HCC cells. HepG2 and PLC/PRF/5 cells also expressed ADAM17, which was clearly knocked down by a siRNA-mediated procedure (Fig. 1*B*).

HepG2 cells and PLC/PRF/5 cells expressed membrane-bound MICA and also produced soluble MICA (Fig. 2*A*). Knockdown of ADAM10 for both cell lines clearly upregulated MICA expression on their cellular surface and downregulated soluble MICA levels in their culture supernatant (Fig. 2*A*). In contrast, knockdown of ADAM17 did not affect the expression of membrane-bound MICA or the production of soluble MICA (Fig. 2*B*). We also examined the involvement of ADAM17 in MICA shedding of phorbol 12-myristate 13-acetate (PMA)–stimulated HCC cells because ADAM17 is considered to primarily affect stimulated shedding. The expression of membrane-bound MICA and the soluble MICA production were equal between PMA-stimulated ADAM17KD-HCC cells and control HCC cells (Supplementary Fig. S2). Thus, ADAM10, but not ADAM17, is critically involved in the shedding of MICA in HCC cells.

We next evaluated the cytolytic activity of NK cells against HCC cells. The cytolytic activity of NK cells against ADAM10KD-HepG2 cells was higher than that against control HepG2 cells. This activity was inhibited by blocking of anti-MICA/B antibody, suggesting that the increase of NK sensitivity depended on the increased expression of membrane-bound MICA on ADAM10KD-HepG2 cells, although we could not exclude the possibility of the involvement of MICB in this cytotoxicity (Fig. 2*C*). Similar results were also obtained with ADAM10KD-PLC/PRF/5 cells.

Epirubicin suppresses ADAM10 expression in HCC cells. We examined the biological modification of human HCC cells by adding epirubicin, which is commonly used in anti-HCC chemotherapy. We first examined the cytotoxicity of epirubicin to human HCC cells by WST-8 assay. Adding >5 μg/mL of epirubicin resulted in a significant decrease in cell growth of both HepG2 and PLC/PRF/5 cells (Fig. 3*B*). Based on these findings, we used 1 μg/mL of epirubicin to evaluate the biological effect on human HCC cells without toxicity. Both HepG2 cells and PLC/PRF/5 cells were cultured for 24 h with epirubicin and then subjected to analysis of ADAM10 expression. Epirubicin suppressed ADAM10 expression at the mRNA and protein levels in both cell lines (Fig. 3*C*). Although the data are not shown, doxorubicin also suppressed ADAM10 expression in HCC cells.

Epirubicin inhibits MICA ectodomain shedding and enhances susceptibility to NK cells of HCC cells. The above observations led us to investigate whether epirubicin or doxorubicin treatment would affect MICA ectodomain shedding in HCC cells. Epirubicin treatment led to an increase in membrane-bound MICA expression and a decrease in soluble MICA production in both HepG2 and PLC/PRF/5 cells (Fig. 4*A*). The mRNA levels of MICA did not change after exposure to epirubicin in both HCC cells (Fig. 4*A*). Similar data were obtained with doxorubicin-treated cells (data not shown).

To confirm whether the soluble MICA detected by ELISA was actually reflected in the cleaved form, we transfected Myc-tagged MICA into HepG2 cells and collected culture supernatants as well as cellular lysates. Immunprecipitates from these samples with anti-Myc were subjected to Western blot analysis after treatment with N-glycosidase. MICA in the culture supernatants migrated faster than cellular MICA (Fig. 4*B*), indicating that the MICA detected by ELISA is actually processed and released from full-length MICA. Epirubicin treatment led to a decrease in soluble MICA protein in HepG2 cells (Fig. 4*B*).

We next evaluated whether the epirubicin treatment could also modify the NK sensitivity of human HCC cells. Epirubicin-treated HepG2 cells or PLC/PRF/5 cells were more susceptible to NK cells than nontreated HepG2 or PLC/PRF/5 cells (Fig. 4*C*). The cytolytic activity against epirubicin-treated HCC cells was significantly decreased to the control levels by adding the anti-MICA/B blocking antibody. These results showed that the addition of epirubicin enhanced the NK sensitivity of HCC cell through increased

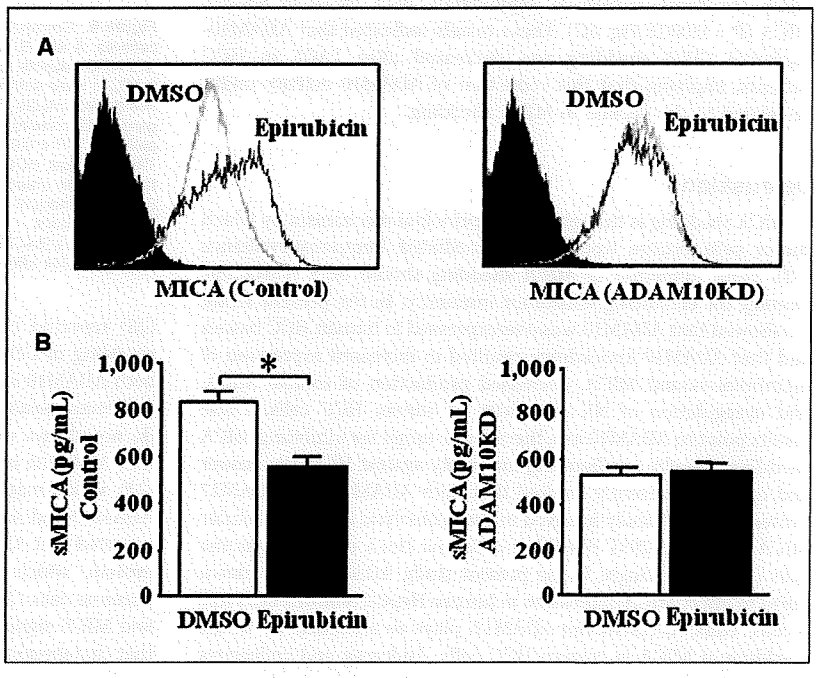

Figure 5. The epirubicin-mediated modification of MICA is ADAM10 dependent. HepG2 cells were transfected with ADAM10 siRNA (*ADAM10KD*) or control siRNA (*Control*) and further cultured with 1 μg/mL of epirubicin (*black lines*) or vehicle (DMSO, *gray line*) for 24 h. The expression of membrane-bound MICA (*MICA*) was evaluated by flow cytometry (*A*), and the soluble MICA (*sMICA*) production in the culture supernatant was evaluated by specific ELISA (*B*). Similar results were obtained from two independent experiments. *, $P < 0.05$.

expression of membrane-bound MICA, although the possibility of MICB involvement could not be excluded. The doxorubicin-treated human HCC cells showed similar results to those obtained from epirubicin-treated HCC cells (data not shown).

Epirubicin inhibits MICA ectodomain shedding through suppression of ADAM10. To examine whether the suppressive effect of epirubicin on MICA shedding occurred through down-regulation of ADAM10, HepG2 cells were transfected with ADAM10 siRNA or scramble siRNA as a control and then treated with epirubicin. Consistent with earlier observations, epirubicin upregulated MICA surface expression and downregulated the levels of soluble MICA in control cells (Fig. 5). In contrast, neither upregulation of surface MICA nor downregulation of soluble MICA levels was observed in ADAM10KD-HepG2 cells. These results suggest that the suppressive effect of epirubicin on MICA shedding is mediated by ADAM10 downregulation. We also found similar results with ADAM10KD-PLC/PRF/5 cells (data not shown).

Soluble CD44 and soluble MICA levels in patients with HCC. We have shown that ADAM10 is expressed in human HCC tissues. However, it is not clear whether ADAM10 activity in HCC tissues is actually involved in MICA shedding in patients. Because ADAM10 was reported to be the constitutive functional sheddase of CD44 (23), we examined the soluble CD44 levels in HCC patients, which might be produced from tumor cells through ADAM10 activity. As shown in Fig. 6*A*, the soluble CD44 levels in HCC patients (n = 97) were significantly higher than those in age-matched healthy volunteers (n = 32). More importantly, soluble MICA levels in HCC patients significantly correlated with soluble CD44 levels (Fig. 6*B*), suggesting a close link between MICA shedding and ADAM10 activity.

We further examined soluble CD44 levels before and 2 weeks after TACE in HCC patients. Whereas the levels did not change in nontreated HCC patients during the 2-week interval (n = 9; 306.7 ± 82.5 ng/mL and 309.9 ± 79.9 ng/mL after 2 weeks), they were significantly decreased in epirubicin-based TACE-treated HCC patients (n = 21; 339.7 ± 78.1 ng/mL before TACE and 308.9 ± 81.4 ng/mL after TACE, P < 0.003). The changes of soluble CD44 in TACE treatment correlated significantly with those of soluble MICA (P = 0.0002; Fig. 6*C*). These results indicated that ADAM10-mediated CD44 shedding was decreased after TACE in HCC patients, implying that this reduction of ADAM10 activity might be related to the decline in MICA shedding.

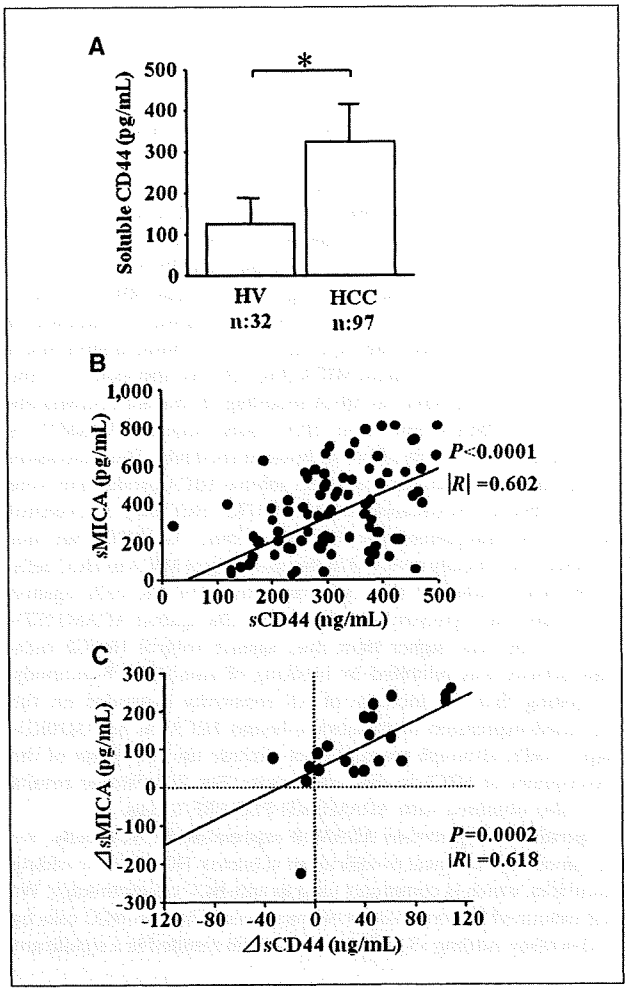

Figure 6. Correlation between soluble CD44 and soluble MICA in human HCC patients. *A* and *B*, soluble CD44 levels and MICA levels in healthy volunteers and HCC patients. Soluble CD44 levels (*sCD44*) and soluble MICA levels (*sMICA*) were determined for sera of HCC patients (n = 97) and age-matched healthy volunteers (*HV*; n = 32). *A*, comparison of sCD44 levels between groups; *B*, correlation between sCD44 levels and sMICA levels in 97 HCC patients. *, P < 0.05. *C*, correlation of sCD44 levels and sMICA levels during TACE therapy. HCC patients (n = 21) treated with epirubicin-based TACE therapy were enrolled and examined for sMICA and sCD44 levels before and 2 wk after therapy. Changes in sMICA (ΔsMICA = serum level of sMICA before TACE treatment − serum level of sMICA after TACE treatment) and those in sCD44 levels (ΔsCD44 = serum level of sCD44 before TACE treatment − serum level of sCD44 after TACE treatment) are plotted.

Discussion

MICA shedding is thought to be a principal mechanism by which tumor cells escape from NKG2D-mediated immunosurveillance (13). Thus, inhibition of MICA shedding should be a reasonable strategy for enhancing antitumor immunity. In the present study, we showed that ADAM10 was overexpressed in human HCC tissues and that ADAM10 knockdown resulted in increased expression of membrane-bound MICA, decreased production of soluble MICA, and upregulation of NK sensitivity of human HCC cells. These results point to ADAM10 as a therapeutic target for inhibiting MICA shedding, thereby ameliorating immunity against HCC. Waldhauer and colleagues recently showed that both ADAM10 and ADAM17 proteases are critically involved in the proteolytic release of soluble MICA of human 293T fibroblast cells and HeLa cervix carcinoma cells (20). Interestingly, in the present study, ADAM17 knockdown failed to affect MICA expression in human HepG2 cells or PLC/PRF/5 cells. Thus, ADAM10, not ADAM17, plays an essential role in the shedding of MICA in human HCC cells. Anderegg and colleagues (23) reported that only ADAM10, not ADAM17, contributed to shedding of CD44 molecules in human melanoma cells although both ADAM10 and ADAM17 proteases were significantly expressed in human melanoma tissues, suggesting that ADAM10 and ADAM17 do not always work in a similar manner. A recent report showed that ADAM10, but not ADAM17, could directly bind to calmodulin (24), which may involve the difference of MICA cleavage between ADAM10 and ADAM17 proteases. Recently, Boutet and colleagues reported that ADAM17 regulates proteolytic shedding of the MICB protein, which is another ligand for the NKG2D receptor on immune cells (25). We previously showed that both soluble MICA and MICB significantly increased in the sera of HCC patients and that therapeutic intervention for HCC leads to reduction of soluble

MICA levels, but not of soluble MICB levels (17), suggesting a more important role of soluble MICA in regulating NKG2D expression after HCC therapy. This led us to focus on the mechanism of MICA shedding in the present study.

Our results revealed that anticancer drugs such as epirubicin and doxorubicin downregulated ADAM10 expression and activity, thereby inhibiting MICA ectodomain shedding. The ADAM family proteins, which are highly expressed in some tumors, play a role in secreting growth factors, such as HB-EGF, and migration of cells. Thus, it is speculated that these proteins could be potential targets for tumor treatment (22). The present study is the first to show that clinically available anticancer drugs have an ability to modulate the expression of ADAM family proteins. They seem to suppress ADAM10 expression at a transcriptional level, but the precise mechanism of this suppression is not yet known.

The MICA ELISA system may not equally detect all soluble MICA (MICA molecules have >60 allelic variants). Our finding that soluble MICA could be detected in all HCC patients suggests that this system was applicable for our cohort of HCC patients. However, special caution should be paid for the use of this ELISA system for widely polymorphic MICA. Because CD44 is well known to be released into circulation from tumors by proteolytic cleavage of ADAM10 (23), the activity of ADAM10 in HCC tissues may be correlated with soluble CD44 levels. If so, our data suggest a close link between ADAM10 activity and the shedding of MICA in HCC. Furthermore, the decline in soluble MICA levels correlated well with the decline in soluble CD44 levels as early as 2 weeks after epirubicin-based TACE therapy. Reducing the tumor volume by such therapy may have led to both decreases but it is also possible that epirubicin suppresses ADAM10 activity, thereby inhibiting the shedding of MICA and CD44. Epirubicin may have a previously unrecognized role in cancer therapy; that is, affecting ADAM10 activity and MICA shedding rather than simply serving as a direct toxic agent for tumor cells.

Our data suggest that anti-HCC chemotherapy could remodel HCC cells, enhancing sensitivity to NK cells by upregulating MICA expression on the cellular surface. A concomitant decline in soluble MICA levels ameliorates NK cell ability by upregulating its NKG2D expression. We previously showed that activation of local innate antitumor immunity in liver tissues resulted in eliciting tumor-specific acquired immunity (21). If liver innate immunity is efficiently activated after anti-HCC chemotherapy, an additional antitumor effect against HCC cells could be expected. Immune modulators such as α-galactosylceramide have been shown to efficiently activate liver innate immune cells, including NK cells (21, 26). The combination therapy of anti-HCC chemotherapy and immunotherapy targeting NK cells might improve the antitumor effect of unresectable HCC and the prognosis of HCC patients.

In spite of recent progress in HCC therapies, there remains significant room for improvement, especially with respect to advanced liver cancer. We have shown here that anti-HCC chemotherapy resulted in enhanced NK sensitivity of HCC cells through inhibition of the activity of ADAM10 protease followed by modification of MICA expression. These findings indicate that efficient activation of liver innate immunity after anti-HCC chemotherapy might represent a particularly promising approach to suppress tumor growth and promote regression in liver cancer patients.

Disclosure of Potential Conflicts of Interest

No potential conflicts of interest were disclosed.

Acknowledgments

Received 3/4/09; revised 7/15/09; accepted 7/24/09; published OnlineFirst 10/13/09.

Grant support: Grant-in-Aid from the Ministry of Education, Culture, Sports, Science and Technology of Japan (T. Takehara) and Grant-in-Aid for Research on Hepatitis and BSE from the Ministry of Health, Labour and Welfare of Japan (N. Hayashi).

The costs of publication of this article were defrayed in part by the payment of page charges. This article must therefore be hereby marked *advertisement* in accordance with 18 U.S.C. Section 1734 solely to indicate this fact.

References

1. Fattovich G, Stroffolini T, Zagni I, Donato F. Hepatocellular carcinoma in cirrhosis: incidence and trends. Gastroenterology 2004;127:S35–50.
2. Bosch FX, Ribes J, Diaz M, Cleries R. Primary liver cancer: worldwide incidence and trends. Gastroenterology 2004;127:S5–16.
3. Takayasu K, Arii S, Ikai I, et al. Prospective cohort study of transarterial chemoembolization for unresectable hepatocellular carcinoma in 8510 patients. Gastroenterol 2006;131:461–9.
4. Doherty DG, O'Farrelly C. Innate and adaptive lymphoid cells in human liver. Immunol Rev 2000;174:5–20.
5. Mehal WZ, Azzaroli F, Crispe IN. Immunology of the healthy liver: old questions and new insights. Gatsroenterology 2001;120:250–60.
6. Bauer S, Groh V, Wu J, et al. Activation of NK cells and T cells by NKG2D, a receptor for stress-inducible MICA. Science 1999;285:727–9.
7. Groh V, Rhinehart R, Secrist H, Bauer S, Grabstein KH, Spies T. Broad tumor-associated expression and recognition by tumor-derived γδT cells of MICA and MICB. Proc Natl Acad Sci U S A 1999;96:6879–84.
8. Jinushi M, Takehara T, Tatsumi T, et al. Expression of MICA and MICB in human hepatocellular carcinomas and their regulation by retinoic acids. Int J Cancer 2003;104:354–61.
9. Wu JD, Higgins LM, Steinle A, Cosman D, Haugk K, Plymate SR. Prevalent expression of the immunostimulatory MHC class I chain-related molecule is counteracted by shedding in prostate cancer. J Clin Invest 2004;114:560–8.
10. Raffaghello L, Prigione I, Airoldi I, et al. Downregulation and/or release of NKG2D ligands as an immune evasion strategy of human neuroblastoma. Neoplasia 2004;6:558–68.
11. Ogasawara K, Lanier LL. NKG2D in NK and T cell-mediated immunity. J Clin Immunol 2005;25:534–40.
12. Coudert JD, Held W. The role of the NKG2D receptor for tumor immunity. Semin Cancer Biol 2006;16:333–43.
13. Groh V, Wu J, Yee C, Spies T. Tumor-derived soluble MIC ligands impair expression of NKG2D and T cell activation. Nature 2002;419:734–8.
14. Salih HR, Rammensee HG, Steinle A. Downregulation of MICA on human tumors by proteolytic shedding. J Immunol 2002;169:4098–102.
15. Salih HR, Antropius H, Gieseke F, et al. Functional expression and release of ligands for activating immunoreceptor NKG2D in leukemia. Blood 2003;102:1389–96.
16. Jinushi M, Takehara T, Tatsumi T, et al. Impairment of natural killer cell and dendritic cell functions by soluble form of MHC class I-related chain A in advanced human hepatocellular carcinoma. J Hepatol 2005;43:1013–20.
17. Kohga K, Takehara T, Tatsumi T, et al. Serum levels of soluble major histocompatibility complex (MHC) class I-related chain A in patients with chronic liver disease and changes during transcatheter arterial embolization for hepatocellular carcinoma. Cancer Sci 2008;99:1643–9.
18. Holdenrieder S, Stieber P, Peterfi A, Nagel D, Steinle A, Salih HR. Soluble MICA in malignant disease. Int J Cancer 2006;118:684–7.
19. Kaiser BK, Yim D, Chow IT, et al. Disulphide-isomerase-enabled shedding of tumor-associated NKG2D ligands. Nature 2007;447:482–6.
20. Waldhauer I, Goehlsdorf D, Gieseke F, et al. Tumor-associated MICA is shed by ADAM proteases. Cancer Res 2008;68:6368–76.
21. Tatsumi T, Takehara T, Yamaguchi S, et al. Intrahepatic delivery of α-galactosylceramide-pulsed dendritic cells suppresses liver tumor. Hepatology 2007;45:22–30.
22. Mochizuki S, Okada Y. ADAMs in cancer cell proliferation and progression. Cancer Sci 2007;98:161–7.
23. Anderegg U, Eichenberg T, Parthaune T, et al. Simon JC. ADAM10 is the constitutive functional sheddase of CD44 in human melanoma cells. J Invest Dermatol 2009;129:1471–82.
24. Nagano O, Murakami D, Hartmann D, et al. Cell-matrix interaction via CD44 is independently regulated by different metalloproteinases activated in response to extracellular domain Ca^{2+} influx and PKC activation. J Cell Biol 2004;165:893–902.
25. Boutet P, Aguera-Gonzalez S, Atkinson S, et al. The metalloproteinase ADAM17/TNF-α enzyme regulates proteolytic shedding of the MHC class I-related chain B protein. J Immunol 2009;182:49–53.
26. Miyagi T, Takehara T, Tatsumi T, et al. CD1d-mediated stimulation of natural killer T cells selectively activates hepatic natural killer cells to eliminate experimentally disseminated hepatoma cells in murine liver. Int J Cancer 2003;106:81–9.